THE CITY COLLEGE
CITY UNIVERSITY OF NEW YORK
NEW YORK, N.Y. 10031

FINAL REPORT

INVESTIGATION OF MODELS FOR LARGE-SCALE METEOROLOGICAL PREDICTION EXPERIMENTS

NASA, Goddard Space Flight Center
Grant NGR 33-016-086
(Supplement No.7)

Jerome Spar, Principal Investigator

31 January 1981

Investigation of Models for Large-Scale Meteorological Prediction Experiments

During the past year the City College group continued its collaboration with the Goddard Institute for Space Studies (GISS) in the investigation of climate simulations generated by the GISS coarse-mesh climate model (Hansen et al., 1980).

Graduate students employed on the project were Zaphiris D. Christidis (through May 1980), Michael Dennis (through June 1980), Charles Cohen and Peter Wu.

Two technical reports have been distributed ("Spherical harmonic analysis of a synoptic climatology generated with a global general circulation model" by Z. D. Christidis, and "Eigenvector analysis of some observed and model-generated climatological fields" by M. Dennis and J. Spar). A paper by J. Spar ("Prediction experiments with a coarse-mesh global model") was published in the Proceedings of the Fourth Annual Climate Diagnostics Workshop, Madison, Wis., October 16-18, 1979, NOAA, pp. 413-423, March 1980, and a paper by Z. D. Christidis and J. Spar ("Spherical harmonic analysis of a model-generated climatology") was accepted for publication in the Monthly Weather Review (February 1981).

The remainder of this report consists of a paper on a series of climate simulation experiments conducted with the coarse-mesh climate model by Spar, Cohen, and Wu for the purpose of better understanding the role of initial and surface boundary conditions on the model-generated climates. At this time only preliminary results of these experiments are available, and statistical evaluations have not yet been carried out. The experiments themselves are still in progress, and will be completed within the next few months.

Climate Simulation Experiments with a Coarse-Mesh General Circulation Model : Preliminary Results

J. Spar, C. Cohen and P. Wu

Introduction

General circulation models (GCM's), including the GISS coarse-mesh (8^{o} x 10^{o}) climate model (Hansen, et al., 1980), are often used to perform "prescribed change" experiments in which some alteration in solar radiation, surface boundary conditions, or atmospheric composition is specified and the atmospheric response, i.e. the effect of the prescribed change on the weather or climate, is calculated. In such experiments, the specified change is usually some small perturbation of the basic constraints on the system, and the computed response of the model may be weaker than the background noise. The analysis of these experiments would undoubtedly be aided by a better understanding of the ways in which the primary climatological controls combine to generate the basic climatic state. In this study, an attempt is made to compute the contributions of various surface boundary conditions to the monthly mean states generated by the 7-layer, 8 x 10 GISS climate model (Hansen et al., 1980), and also to examine the influence of initial conditions on the model climate simulations.

For the purposes of the study, such obvious climatic controls as the shape and rotation of the earth, the solar radiation, and the dry composition of the atmosphere are fixed, and only the surface boundary conditions are altered in the various climate simulations. The model (version 660) is operated at a fixed solar declination, specifically that of January 15, initialized on January 1, and allowed to simulate 15 or more successive Januaries without going through the annual cycle. Monthly means are computed for each January and for ensembles of all but two (or more) Januaries, the first two (or more) months being discarded as transients.

The model is initially forced by the sea-surface temperature (SST) field alone (plus, of course, rotation, etc.) by eliminating all land and specifying a zonally uniform SST pattern with the value at each grid latitude equal to the zonal average of the climatological monthly mean SST, but with sea ice caps (3m thick) over the Arctic and Antarctic. For this "water planet" experiment (001), the model was first initialized with monthly mean zonal values of the atmospheric history variables, including winds, taken from an earlier 5-year model climate simulation (Christidis and Spar, 1980), except for the surface pressure which was assigned a globally uniform initial value of 1010 mb. This initialization was adopted for the purpose of reducing the "spin up" time in the experiment on the assumption that the model would soon "forget" its initial conditions and adjust rapidly to the boundary conditions. However, early results of the experiment indicated an apparent tendency for persistence of the initial state (except for a redistribution of the surface pressures and some alterations of the winds), probably as a consequence of the constancy of the forcing, the absence of an annual cycle, and the zonal symmetry of the surface boundary conditions. Indeed, as shown below, there was enough similarity between the initial state and the model-generated climate in this perpetual January "water planet" experiment that the possibility of initial conditions having a dominating influence on the model-generated climate could not be ignored. It was therefore deemed necessary, after all, to conduct a "water planet spin up" experiment (000) in which the model is initialized with globally uniform mean values of sigma-level specific humidities and temperatures, as well as a constant surface pressure and zero winds.

Following the two water planet experiments, flat continents are placed on the earth, with zero elevation above sea level, zero water storage capacity, and uniform surface albedo, in order to assess the thermal influence of the land, while the zonal distribution of sea ice

and SST remain unchanged over the oceans. The model is again initialized with the same state of rest as in the water planet spin up experiment, and is again run for a period of at least 15 Januaries, the first 2 (or more) months being discarded. The initial surface albedo of Greenland and Antarctica is that of glacial ice, but snow is allowed to alter both the sea ice and continental albedos as computed by the model. The climatic effects of the flat dry continents as heat sources and sinks may then be evaluated by comparing the "flat continent" model climatology (002), computed by averaging all but the first 2 or more Januaries, with that of the water planet (000).

The effect of mountains on the global model climatology is computed by repeating the last run, but with the correct model terrain elevation restored at each grid point. However, in the "mountain" experiment (003) the model is initialized not only with a state of rest, but also with a completely dry and isothermal atmosphere, so that it is required to generate its own humidity and temperature distribution. The ground albedo is still kept uniform over the continents, except where snow is calculated, and the water storage capacity is zero in this mountain run.

The climatic effects of variable surface albedo and water storage capacity over the continents are investigated through a second perpetual January mountain experiment (004) with the model, while the influence of departures from zonal symmetry of the SST field is examined by comparing the results of the previous run with the perpetual January climatology generated by the complete model using the actual January climatological SST's.

This report presents some preliminary results of the experiments conducted thus far. A more complete analysis of experimental results, including statistical evaluation, will be reported later.

Experiments with a zonally symmetric water planet

In the first of the two water planet experiments (001) the coarse mesh 7-layer model was initialized with zonal mean values of temperature, humidity, and wind for the month of January derived from an earlier model climate simulation based on 5 annual cycles, but with a constant surface pressure (1010 mb). During the first month of the simulation, a rapid mass redistribution occurs, undoubtedly in response to the initial wind field. The 13-year mean meridional distribution of surface pressure (P_s, in mb) shown in Fig. 1 evolves quickly, with a near-equatorial low, subtropical or mid-latitude highs, subpolar lows, and an Antarctic high. At the same time, the zonal wind distribution undergoes a moderate alteration, as illustrated in Fig. 2, which shows the meridional profiles of the mean zonal wind ($\bar{U}$, in ms^{-1}), integrated over the 7 layers of the model, both in the initial state (dashed) and as generated by the model and averaged over the last 13 Januaries (solid). Within the first 2 months of the simulation, the tropical easterlies, which initially extend from 8N to 23S, shrink to the zone 8N to 8S and diminish in speed, while the strongest westerlies, initially located at 47N and 39S, shift closer to the Equator and stabilize as shown in Fig. 2.

The meridional wind component (V) also changes as shown in Fig. 3 illustrating the meridional profiles of V in the lowest layer of the model (V_1, in cm S^{-1}) both as given in the initial conditions (dashed) and as generated by the model and averaged over the last 13 Januaries (solid). Initially, maximum low-level northerly (negative) winds are centered near 20N, while the strongest southerly (positive) winds appear at 31S, with a secondary southerly maximum at the Equator and an apparent double intertropical convergence (ITC). Within one month the northerly maximum shifts equatorward and the principal southerly maximum moves to the Equator and amplifies, producing one dominant ITC at 4N as shown in Fig. 3. The resulting distribution of vertical

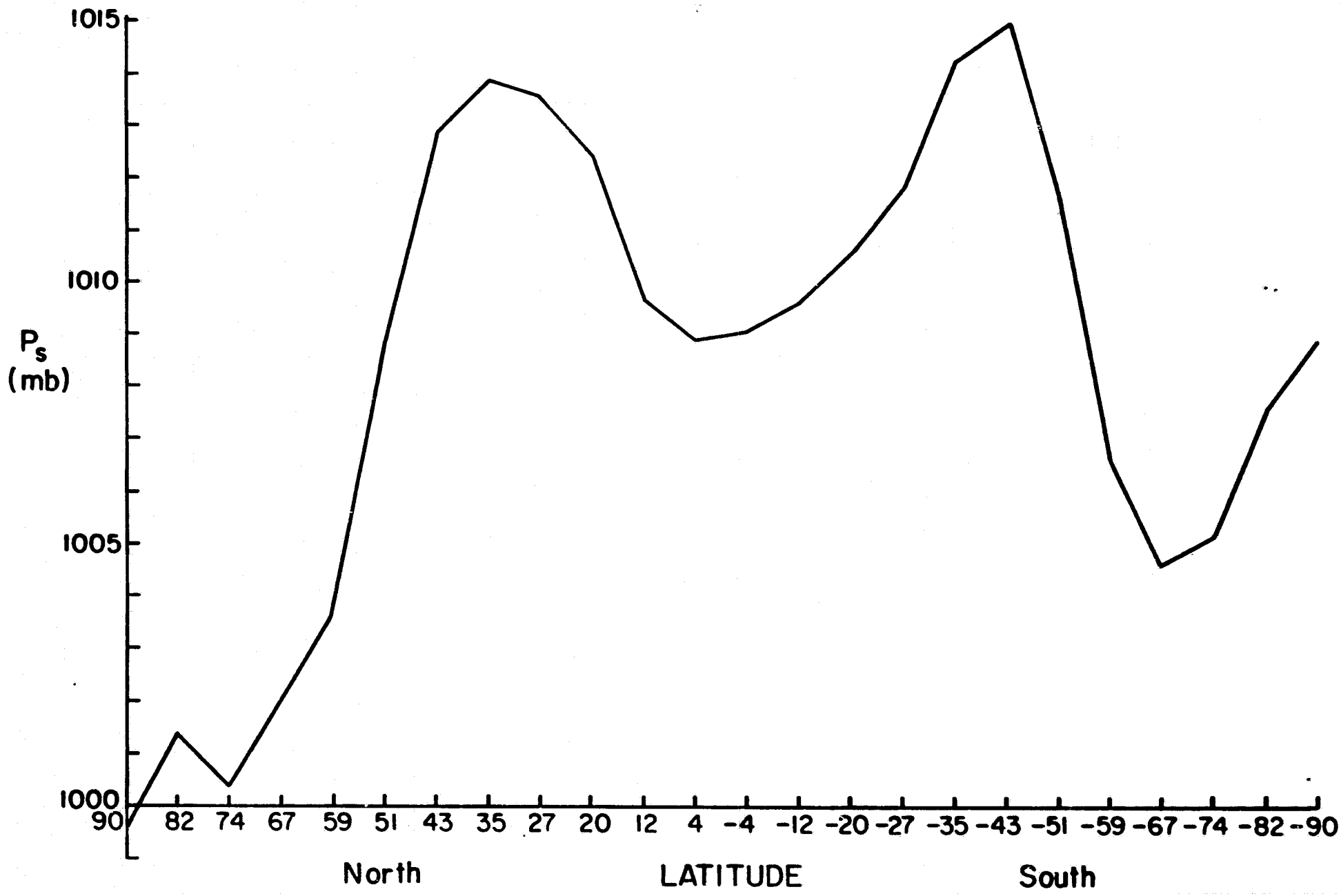
1015
1010
1005
1000
P_s
(mb)
90
82
74
67
59
51
43
35
27
20
12
4
-4
-12
-20
-27
-35
-43
-51
-59
-67
-74
-82
-90
North
LATITUDE
South

Fig. 1

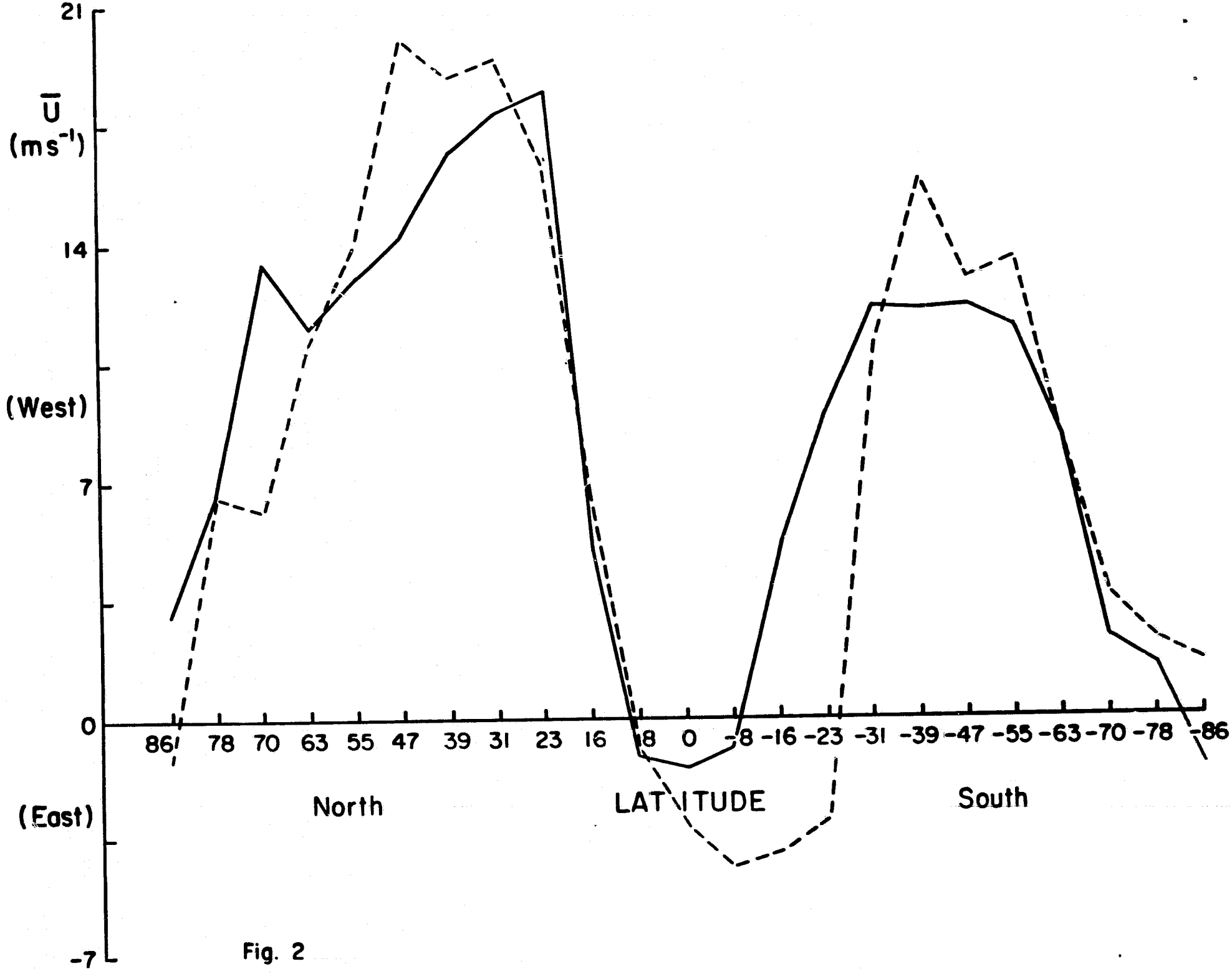
21
$\overline{U}$
(ms^{-1})
14
(West)
7
0
(East)
-7
86
78
70
63
55
47
39
31
23
16
8
0
-8
-16
-23
-31
-39
-47
-55
-63
-70
-78
-86
North
LATITUDE
South

Fig. 2

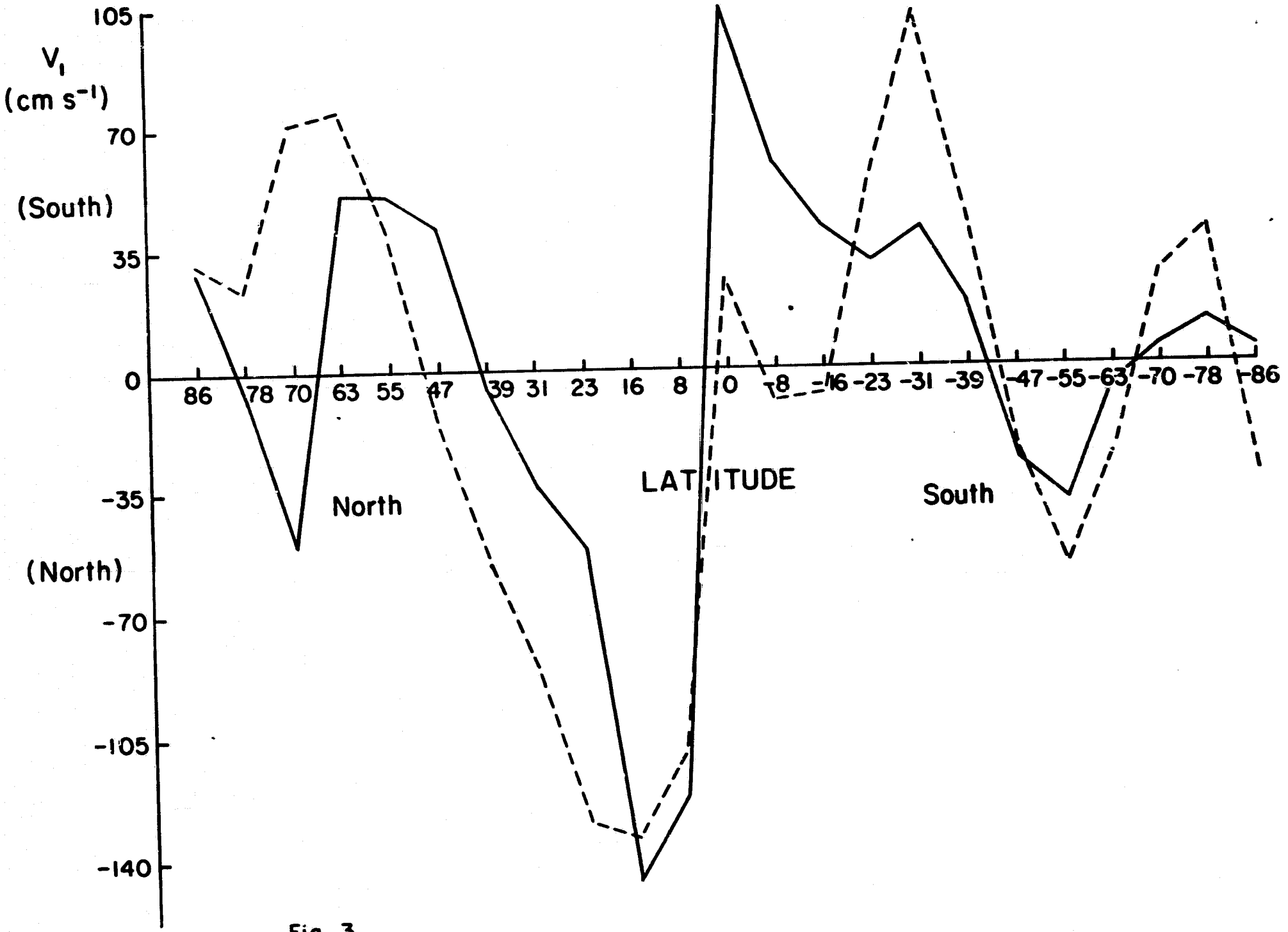
105
V_1
(cm s^{-1})
70
(South)
35
0
-35
(North)
-70
-105
-140
86 78 70 63 55 47 39 31 23 16 8 0 -8 -16 -23 -31 -39 -47 -55 -63 -70 -78 -86
North
LATITUDE
South

Fig. 3

velocity ($\bar{W}$, in mm S^{-1}), integrated over the 7 layers of the model and averaged over the last 13 Januaries, is shown in Fig. 4, where the maximum upward (positive) motion at 4N is the dominant feature and the cause of a precipitation maximum. Also noted in Figs. 3 and 4 is the fact that, although latitude 20N is initially the location of the belt of strongest northerly winds (the northeast trades), and hence almost zero vertical motion, the model generates maximum divergence, and hence maximum subsidence, at that latitude, completing a Hadley circulation that develops in the first month. Another radical alteration of V_1 is seen in Fig. 3 in the Arctic, where an initially southerly wind at 70N reverses (again in the first month) and remains northerly in the 13 January average.

Deviations from initial conditions are somewhat less dramatic in the vertical distributions of wind and temperature. In Fig. 5, showing vertical profiles of the initial and 13 year average model-generated zonal winds (U) at latitudes 39N and 39S, plotted against pressure (P) on a logarithmic scale, the model exhibits a marked decrease in the westerlies. The lapse rate of temperature (not shown), on the other hand, exhibits very little change from the initial state at all latitudes, except over the open ocean south of the Arctic ice cap where the surface air temperatures rises quickly from an initial value of - 25C to the water temperature of - 1C.

As expected from the zonal symmetry of both the initial atmospheric state and the surface boundary conditions, the horizontal fields of the model-generated climatic variables display mainly a zonally symmetric character when averaged over 13 Januaries, although waves and cells are found on the individual January maps. For example, the third mean January sea-level pressure field computed by the model (Fig. 6) exhibits two or three distinct Arctic lows and three or four subtropical high cells in the Northern Hemisphere. However, the 13-month mean Jaunary field of sea-level pressure in Fig. 7 is predominantly zonal, as are those of the layer temperatures for 850-1000 mb and 700-850 mb (Figs. 8 and 9) and the geopotential heights of the 700 mb and 500 mb surfaces (Figs. 10 and 11). The last four fields, in fact, remain nearly constant during the 15 months of the perpetual January simulation.

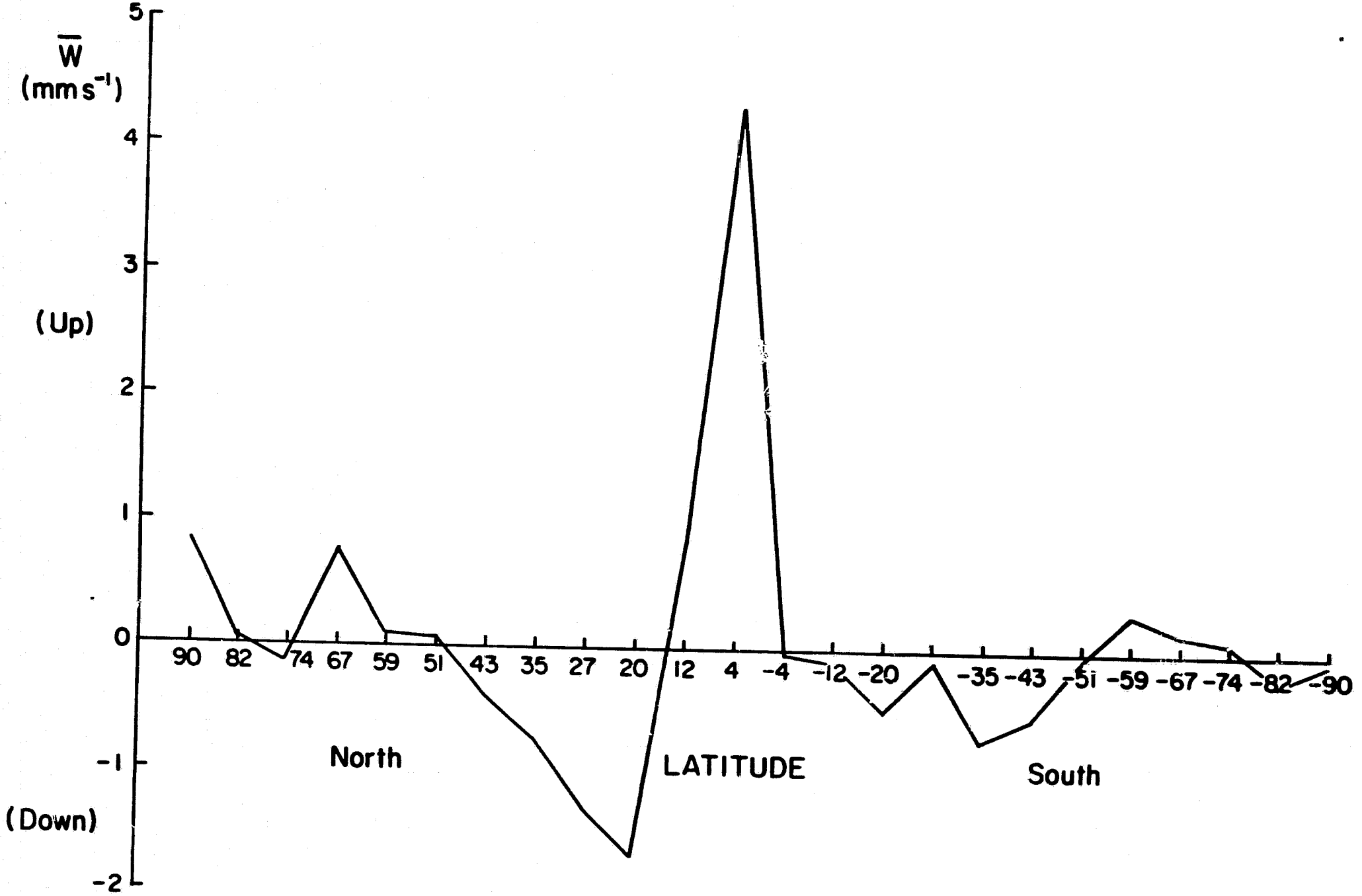
5
$\overline{W}$
(mm s^{-1})
4
3
(Up)
2
1
0
-1
(Down)
-2
90 82 74 67 59 51 43 35 27 20 12 4 -4 -12 -20 -35 -43 -51 -59 -67 -74 -82 -90
North
LATITUDE
South

Fig. 4

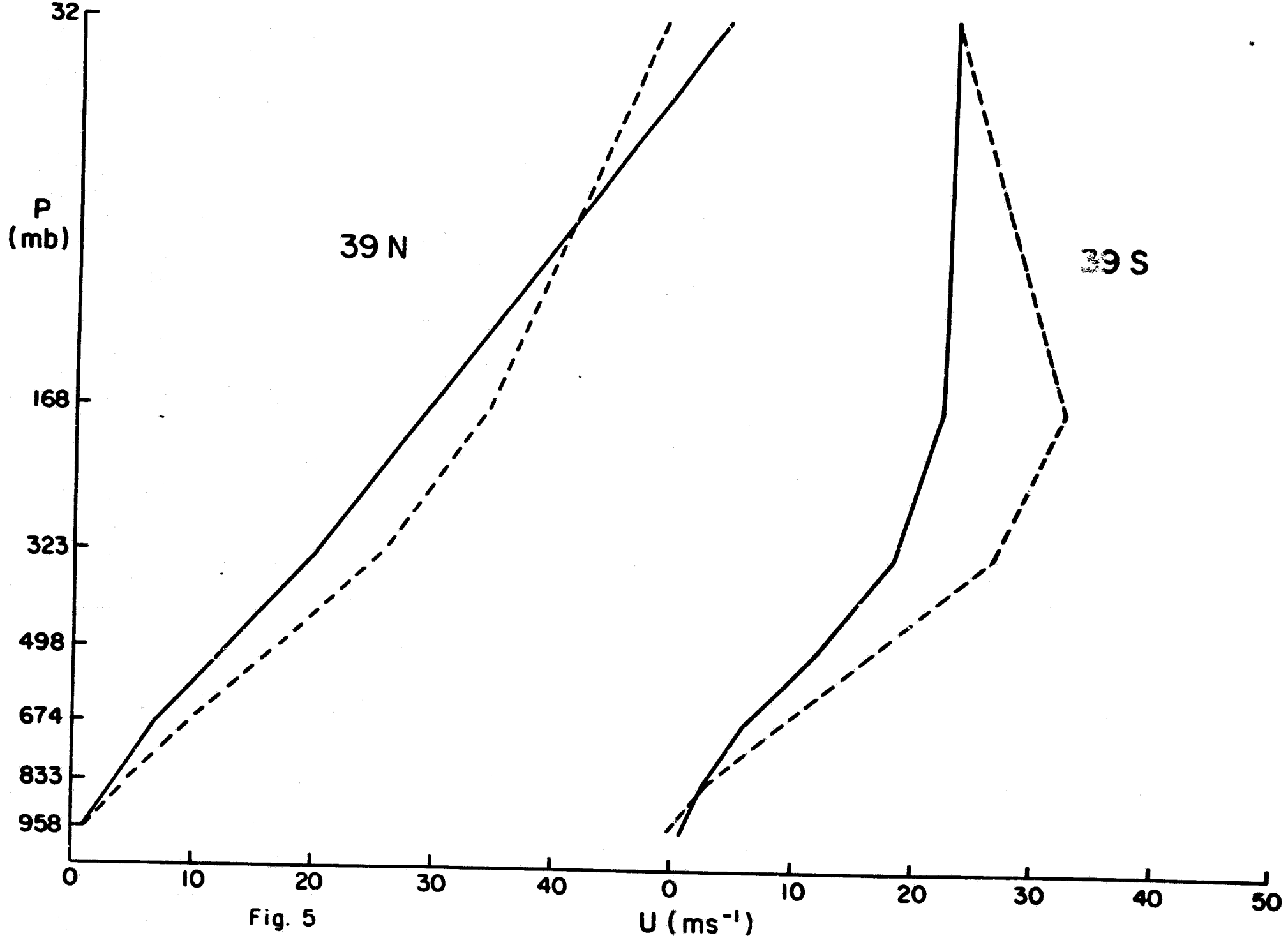
32
P
(mb)
168
323
498
674
833
958
39 N
39 S
0
10
20
30
40
0
10
20
30
40
50
U (ms⁻¹)

Fig. 5

DAY 61. HR 0 (1 M3 1900) 1440.0 TO DAY 91. HR 0 (1 M4 1900) 2160.0 DIF 720.0 HR

SEA LEVEL PPESSURE (MB)

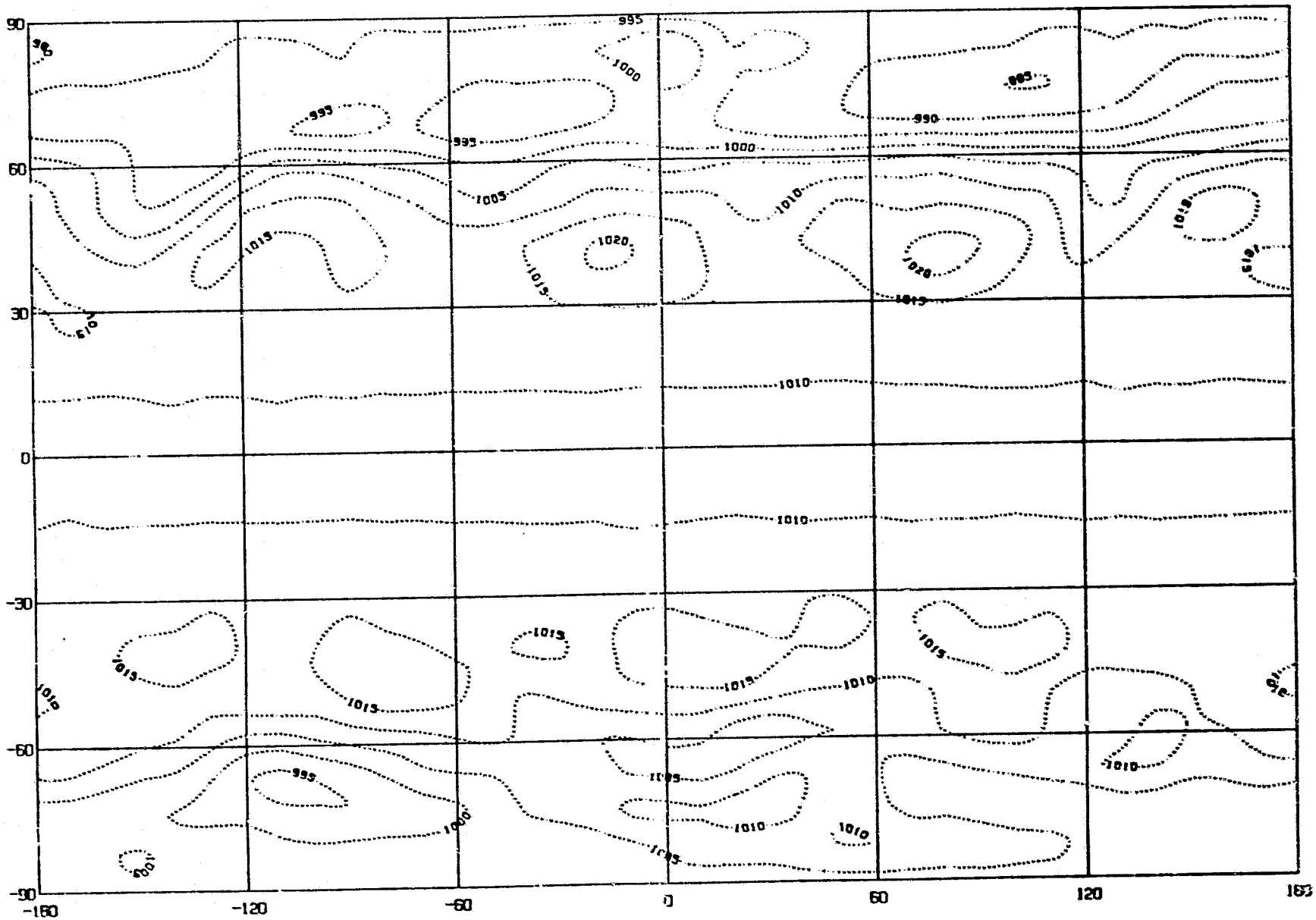

Fig. 6

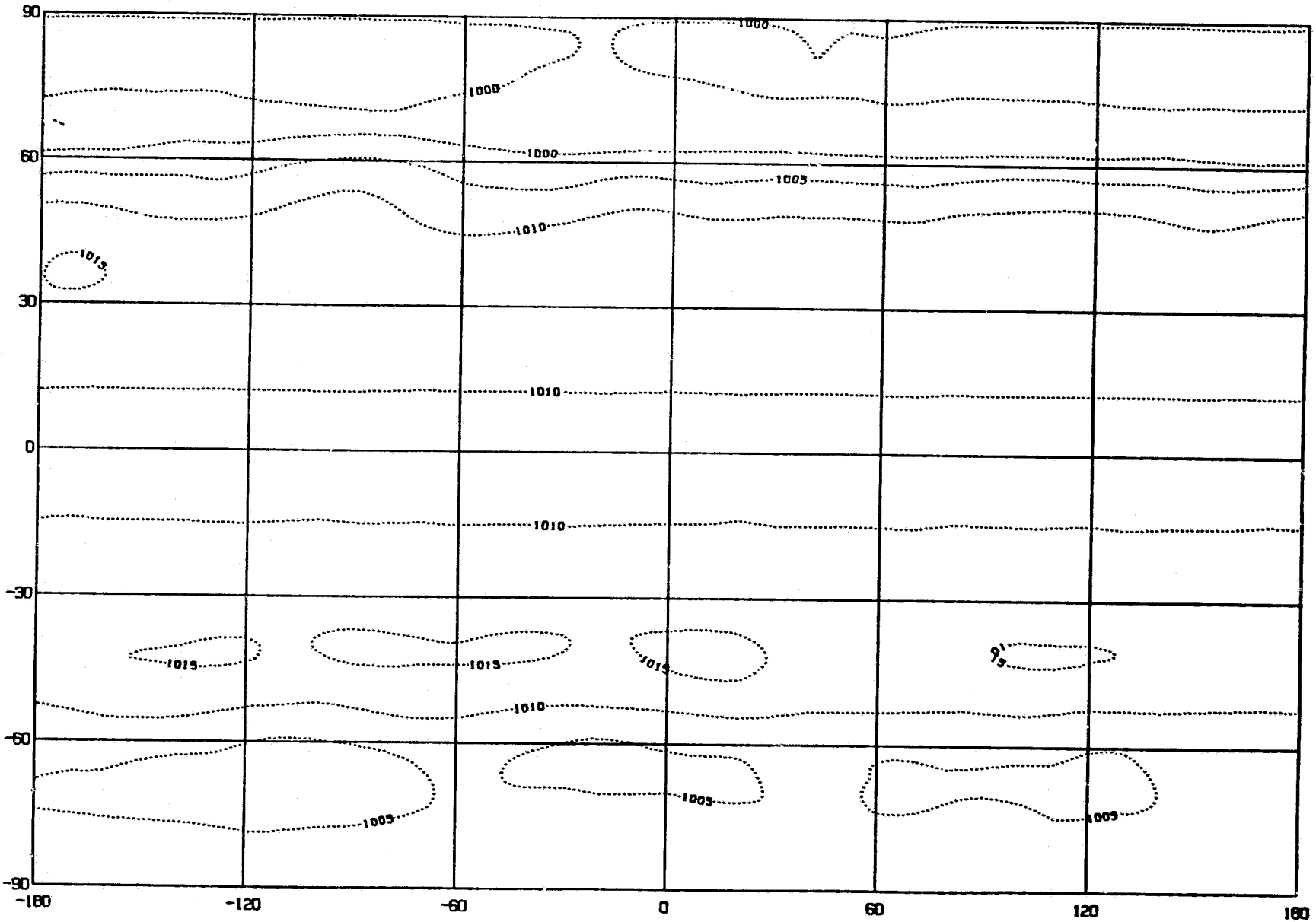

MEAN SEA-LEVEL PRESSURE OF LAST 13 MONTHS

Fig. 7

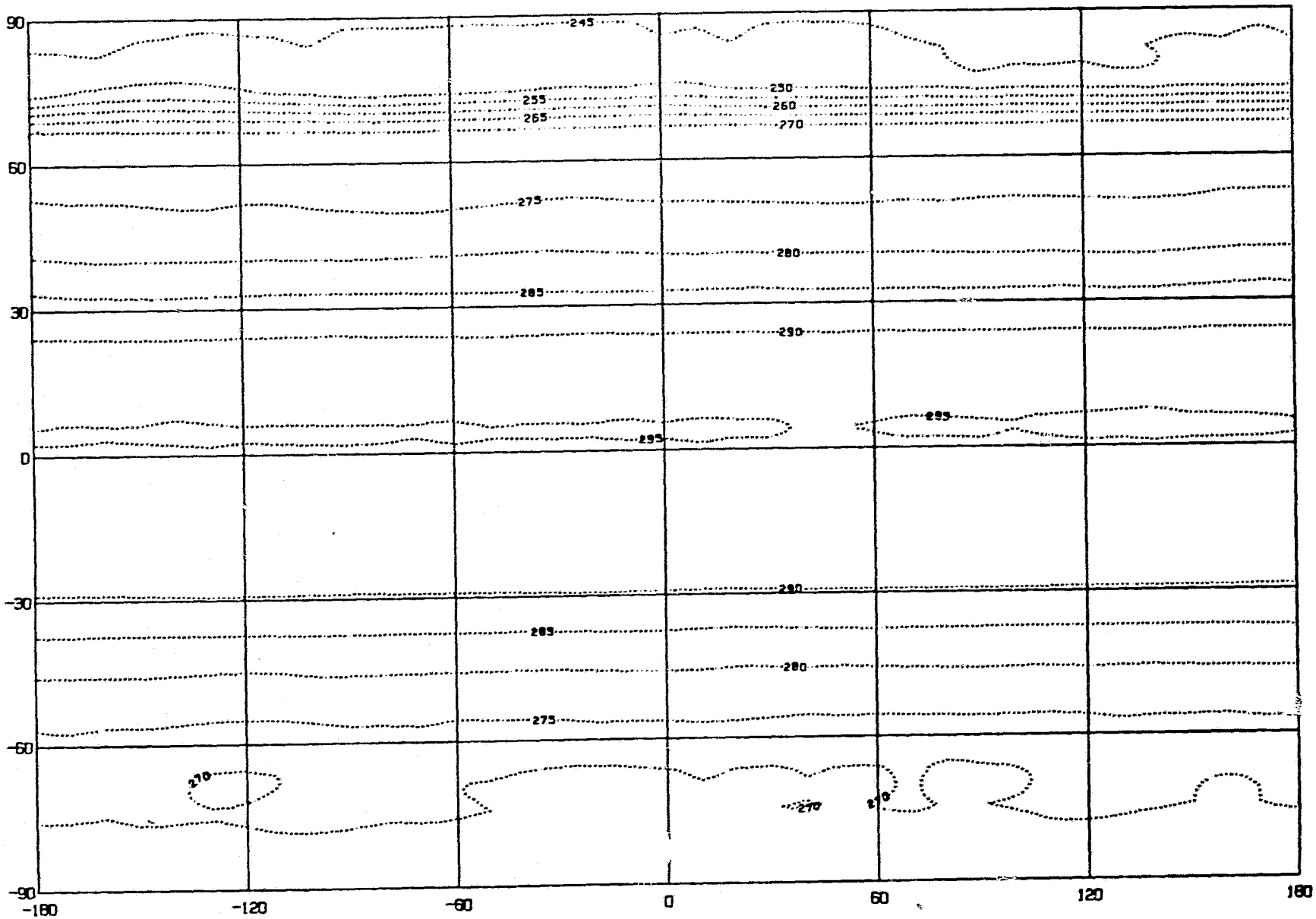

MEAN THICK. TEMP 850-999 OF LAST 13 MONTHS

Fig. 8

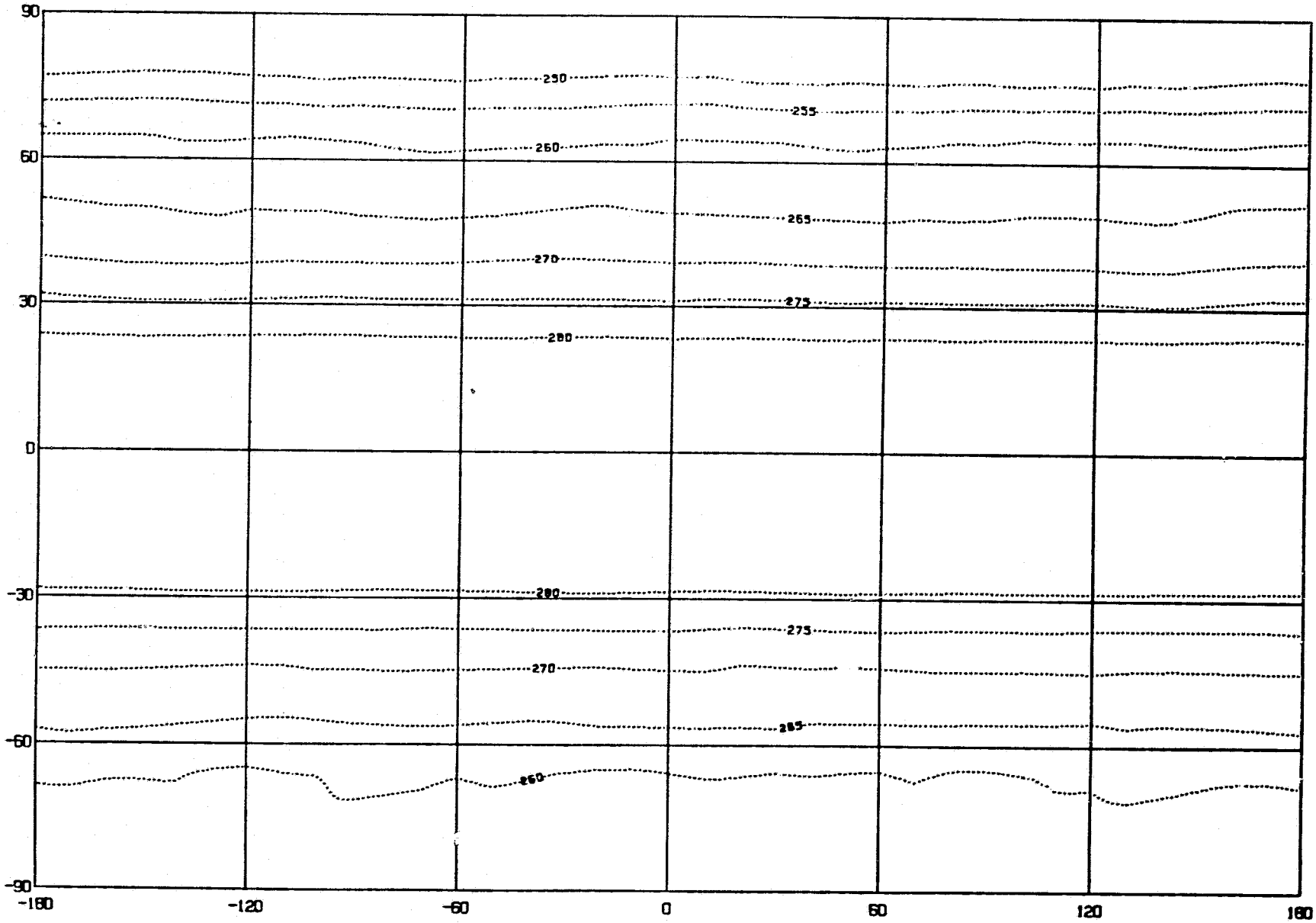

MEAN THICK.TEMP 700-850 OF LAST 13 MONTHS

Fig. 9

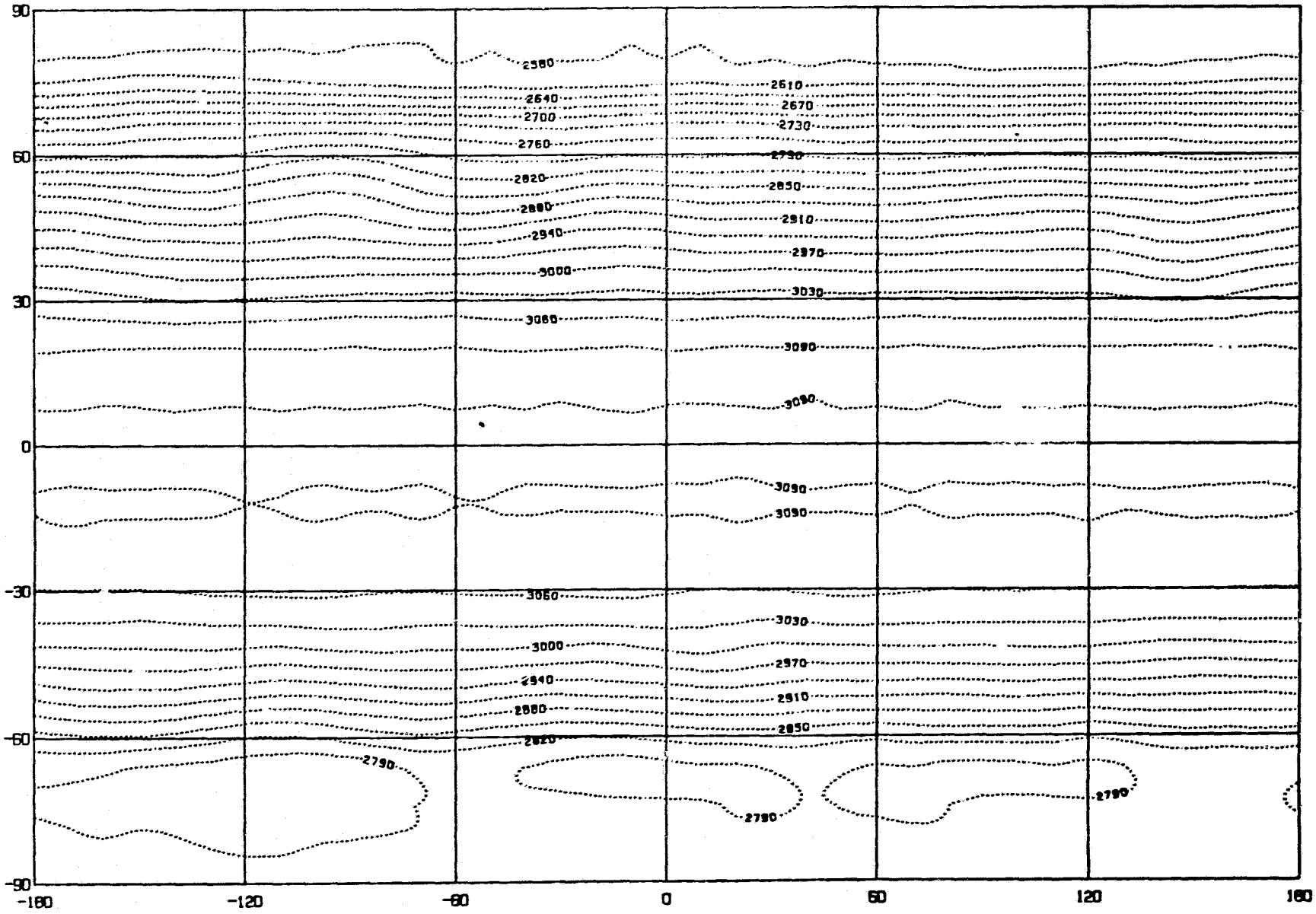

MEAN 700MB HT. OF LAST 13 MONTHS

Fig. 10

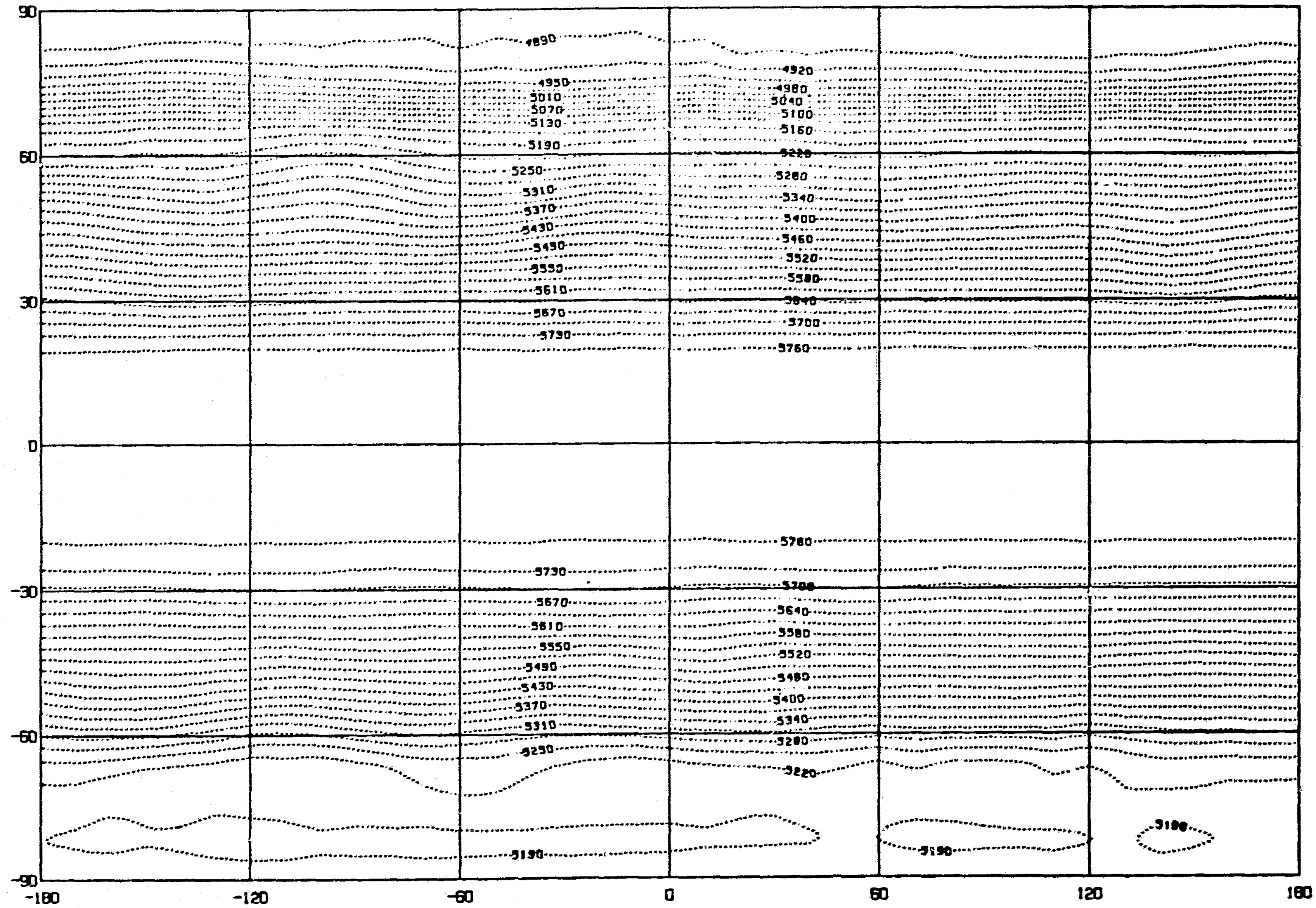

MEAN 500MB HT.OF LAST 13 MONTHS

Fig. 11

Mean meridional cross-sections of temperature (T) and zonal wind (U) for the 15th month of the first January water planet experiment, shown in Figs. 12 and 13, exhibit some of the defects of the model simulation. The tropical tropopause is too low and too warm, the Arctic tropopause is too high and too cold, and the subtropical jet in the Northern Hemisphere is much too high. However, the tropospheric structure of the model atmosphere is not unrealistic.

While there are clearly significant departures of the model-generated winds and pressures from the given initial conditions, there also appears to be considerable persistence of the basic atmospheric structure and circulation, albeit in a modified form. Furthermore, it appears likely that the alterations of winds and surface pressures computed by the model may be due largely to the initial inconsistency between the given wind field and the constant surface pressure, as indicated by the rapid mutual adjustment of these two fields. Thus, there is still a question as to what the model-generated climate would be if the simulation were initialized with a different set of initial conditions, or even allowed to "spin up" from a state of rest. To answer this question, the water planet model was reinitialized with a set of constant temperatures and specific humidities at each level (specifically, the global averages of the initial 5-year model climatology), the same constant surface pressure as before, and zero winds. Again the model was run for 15 months in the perpetual January mode, and the output was averaged over the last 13 Januaries.

The initial adjustment of the model atmosphere in the "water planet spin up" experiments (000) can be described briefly in terms of the mean state for the first month. Surface air temperatures quickly approach the SST's over the open ocean, while in the Arctic both the sea ice and surface air cool to about -10° C. At all tropospheric levels a realistic meridional temperature gradient begins to emerge, while in the stratosphere temperatures increase monotonically from

DAY 421. HR 0 (1 M3 1901) 10080.0 TO DAY 451. HR 0 (1 M4 1901) 10800.0 DIF 720.0 HR

TEMPERATURE (DEGREES CENTIGRADE)

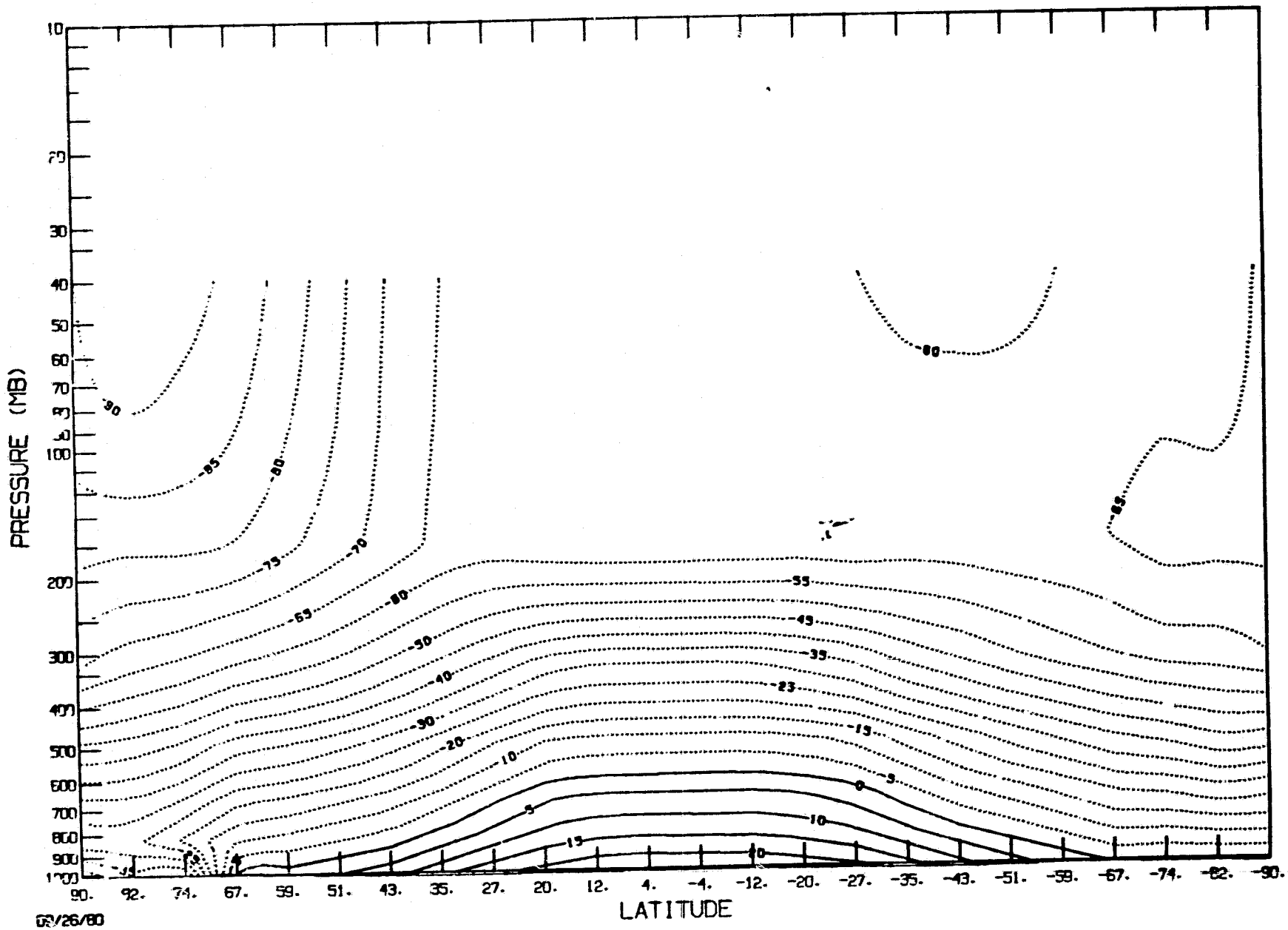

Fig. 12

DAY 421. HR 0 (1 M3 1901) 10080.0 TO DAY 451. HR 0 (1 M4 1901) 10800.0 DIF 720.0 HR

ZONAL WIND (U COMPONENT) (TENTHS OF METERS/SECOND)

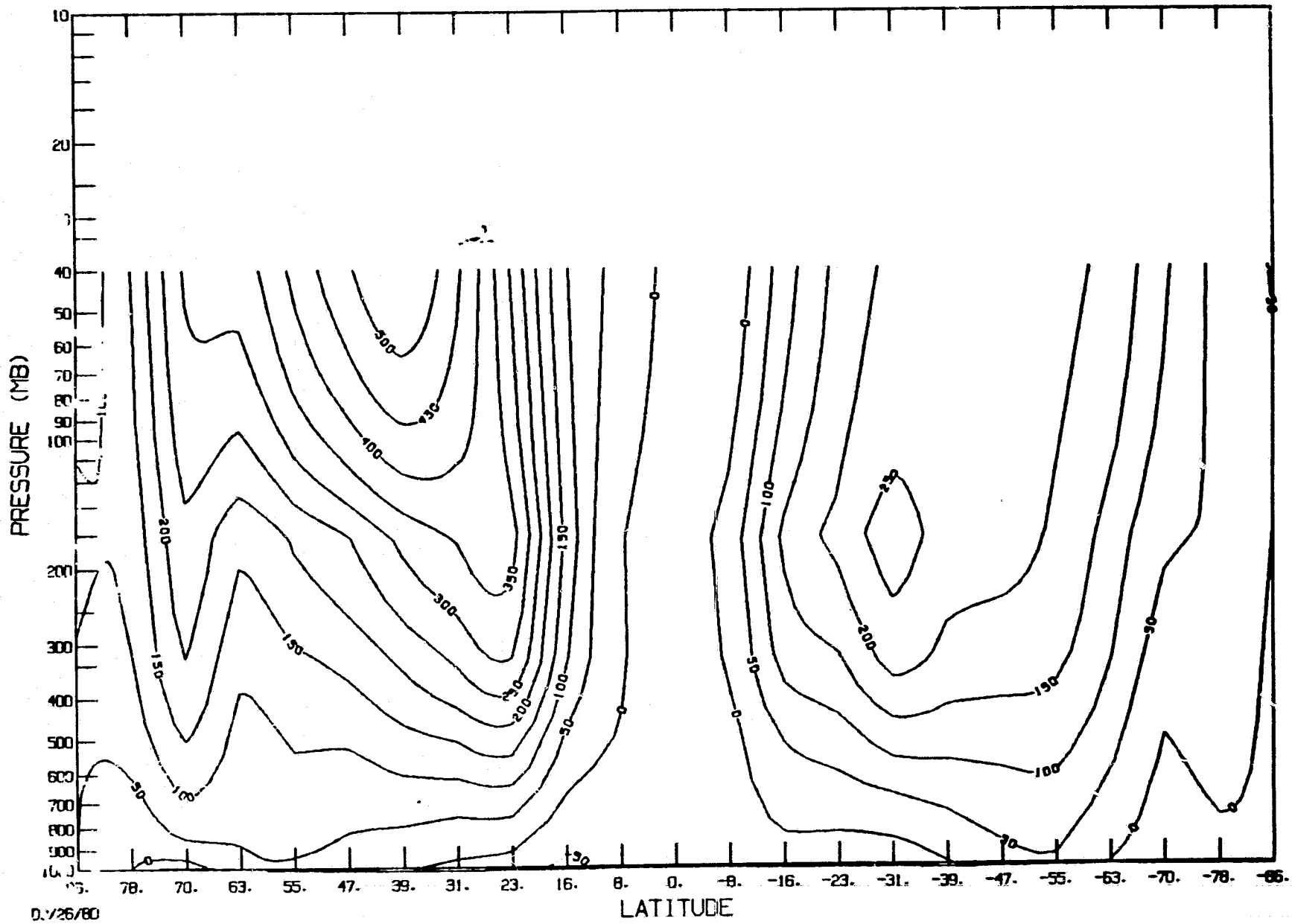

D.Y26/80

Fig. 13

North Pole to South Pole. A realistic meridional gradient of specific humidity begins to appear in the lower troposphere, with very high relative humidities in the lowest layer (nearly saturated conditions poleward of latitude 50 degrees) and considerable cloudiness (more than 70 percent total cloud cover) in the polar regions, with a secondary maximum of cellular cloudiness at the Equator, but little cloud cover in the tropics and subtropics. Surface easterlies appear at all latitudes from 70N to 47S, except at the Equator, with northeast and southeast trade winds centered at 20N and 27S, respectively, and an ITC at 4N, where a mean upward vertical velocity of 4.5 mm s^{-1} closely resembles that found in the first experiment. The westerlies aloft show maxima at 31N and 31S (28 and 22 ms^{-1}, respectively) at level 6 of the model (nominal pressure, 168 mb). The sea-level pressure field displays an equatorial low of less than 1002 mb with bands of high pressure (1024 and 1019 mb) at high latitudes (78N and 55S) in both hemispheres. In middle latitudes, especially in the Northern Hemisphere, both the sea-level pressure field (Fig. 14) and the surface winds exhibit large amplitude waves in the first month.

Within the next few months, the mean January states generated by the model in the water planet spin up computation rapidly approach the 13-January mean of the first water planet experiment. The evolution of the surface pressure profile, for example, as illustrated in Fig. 15, shows the change over the first 3 Januaries (see numbers on curves) from an initially constant value of 1010 mb to the familiar planetary pressure profile, including the equatorial low, subtropical high cells, and subpolar lows in both hemispheres.

When averaged over the last 13 Januaries, the meridional profiles of P_s, $\bar{U}$, V_1, and $\bar{W}$ for the spin up experiment (not shown) are virtually identical to those shown in Figs. 1-4. The corresponding mean vertical profiles of U (e.g., Fig. 5) and T are also nearly identical in the two climatologies, so that graphs of the results from the two

THIS IS THE 000RUN (WATER SPHERE) WITH MEAN GLOBAL TEMP . SPEC..HUMIDITY.....SPAR.COHEN.WU:RUN#0
DAY 1. HR 0 (1 M1 1900) 0.0 TO DAY 31. HR 0 (1 M2 1900) 720.0 DIF 720.0 HR

SEA LEVEL PRESSURE (MB)

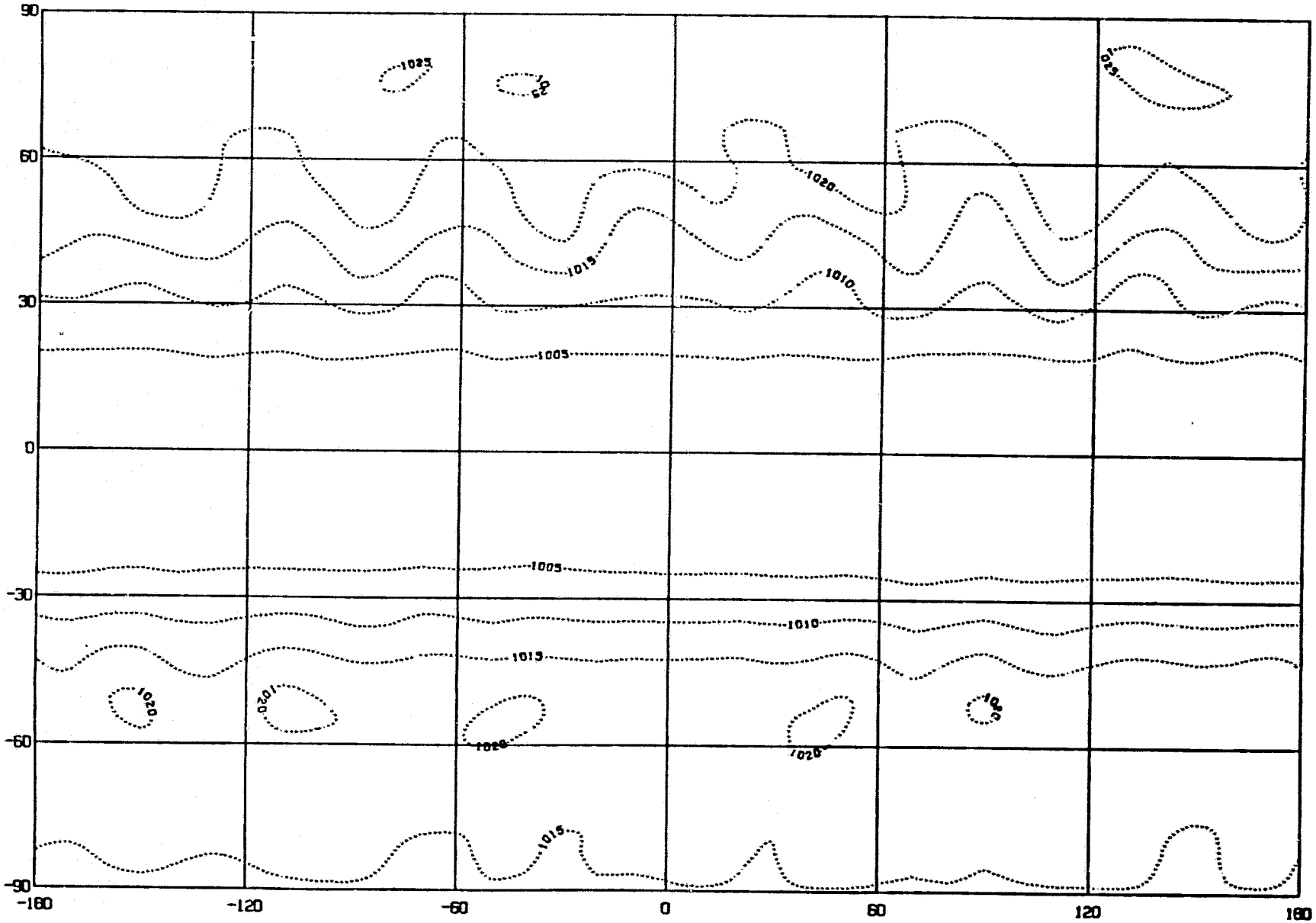

Fig. 14

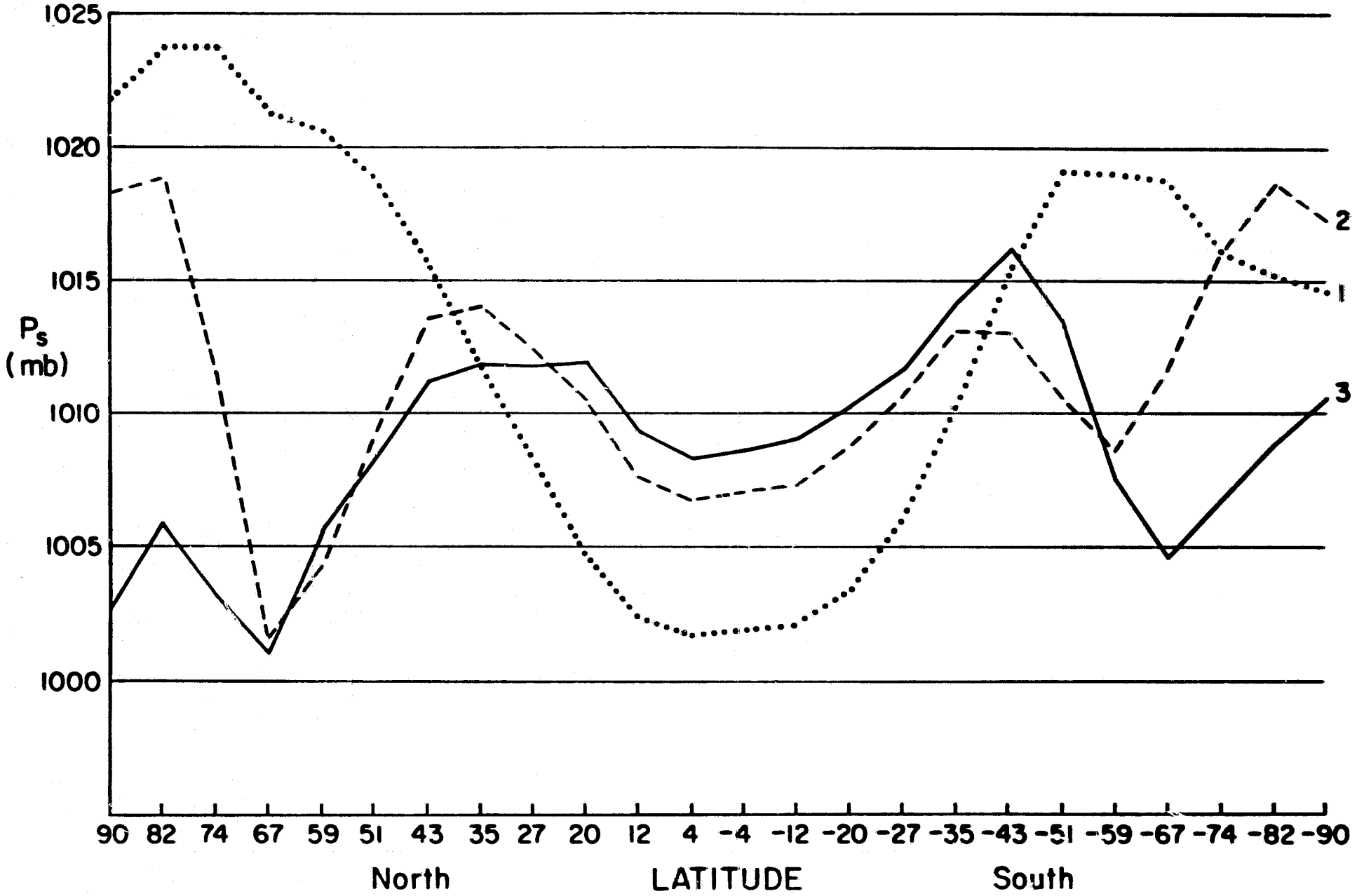
1025
1020
1015
1010
1005
1000
Ps
(mb)
1
2
3
90 82 74 67 59 51 43 35 27 20 12 4 -4 -12 -20 -27 -35 -43 -51 -59 -67 -74 -82 -90
North
LATITUDE
South

Fig. 15

water planet experiments plotted on the same diagram would almost coincide. The 13-January mean synoptic patterns from the spin up experiment (see e.g., the sea-level pressure field shown in Fig. 16) are also almost indistinguishable from the corresponding fields from the first water planet run.

There are, of course, certain differences between the two water planet climatologies which can be seen by comparing Figs. 12 and 13 with Figs. 17 and 18, which show the corresponding 15th January meridional cross-sections of T and U for the spin up run. The two temperature cross-sections are almost identical, but there are some differences between the two wind patterns. Despite these small residual differences, it does appear from the two water planet experiments that the model-generated climate is virtually independent of the initial state. Furthermore, the adjustment time in the spin up experiment was found to be so short that a horizontally uniform state of rest was adopted as the initial condition for the remaining perpetual January runs.

Flat continents experiment (002)

For the next phase of the experiment, geographically realistic but topographically flat continents, with zero water storage capacity, uniform roughness length (0.3 m) and uniform albedo (0.14), were superimposed on the water planet.

A troublesome problem with all perpetual January experiments is the accumulation of snow in the Northern Hemisphere, both on sea ice and on land, wherever the surface temperature is less than 0° C. In the January water planet computation, snow did, in fact, accumulate from month to month, but only over the sea ice in the Northern Hemisphere. The snow line in that case was constrained from advancing southward by the fact that the sea ice limit in all these experiments is arbitrarily fixed. However, no such constraint exists in the model on the continental snow line, and, without an annual cycle to provide for the melting of snow, it was anticipated that continental glaciation over the Northern Hemisphere might spread toward the Equator. A 15-January run with the flat continent model did indeed indicate such

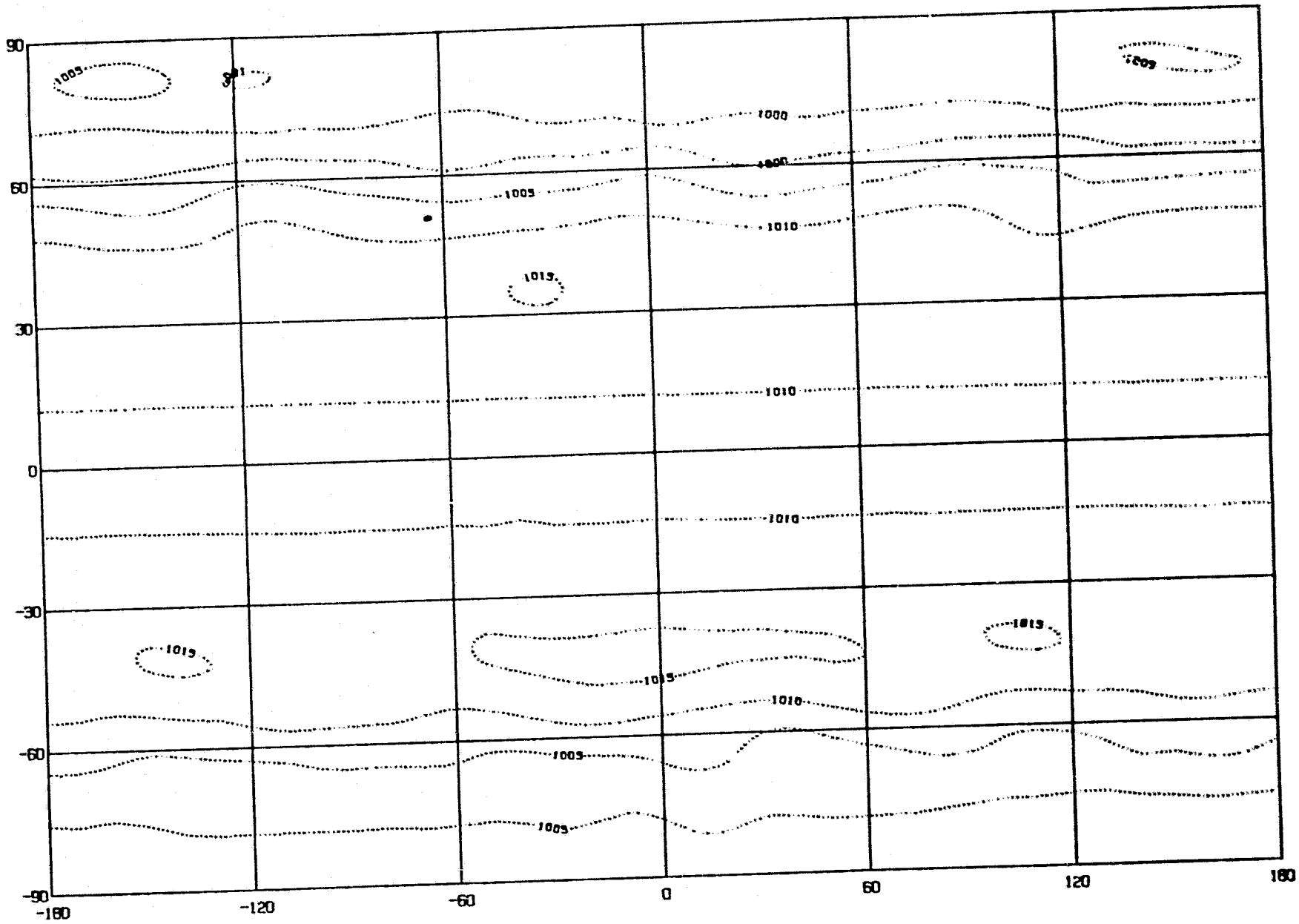

SEA LEVEL PRESSURE OF RUN000 FROM ALL 13 MONTHS MEAN (IN MB.)

Fig. 16

THIS IS THE OOORUN (WATER SPHERE) WITH MEAN GLOBAL TEMP . SPEC..HUMIDITY.....SPAR.COHEN.MU:RUN#0
DAY 421. HR 0 (1 M3 1901) 10080.0 TO DAY 451. HR 0 (1 M4 1901) 10800.0 DIF 720.0 HR

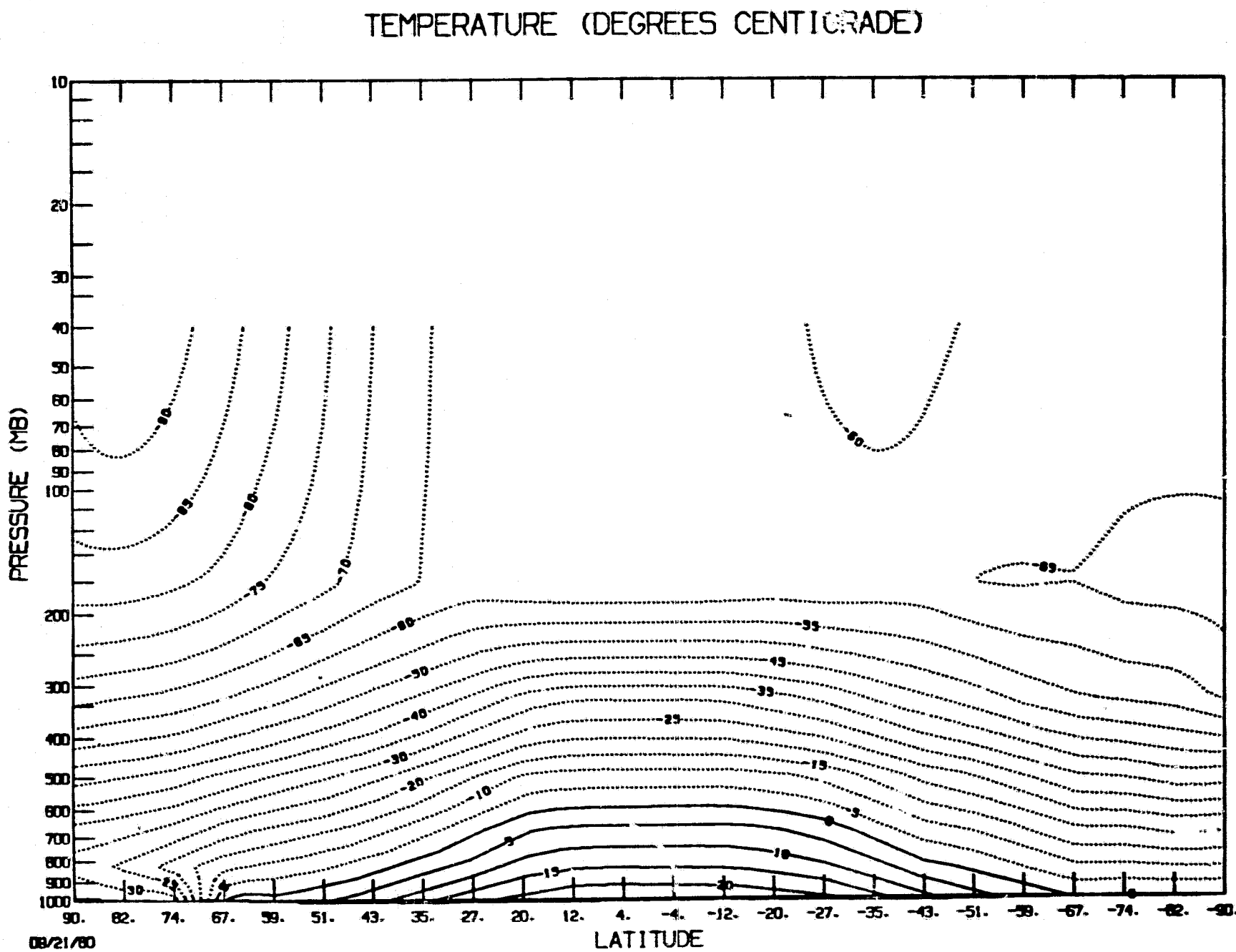

Fig. 17

THIS IS THE 000RUN (WATER SPHERE) WITH MEAN GLOBAL TEMP . SPEC..HUMIDITY.....SPAR.COHEN.WU:RUN#0
DAY 421. HR 0 (1 M3 1901) 10080.0 TO DAY 451. HR 0 (1 M4 1901) 10800.0 DIF 720.0 HR

ZONAL WIND (U COMPONENT) (TENTHS OF METERS/SECOND)

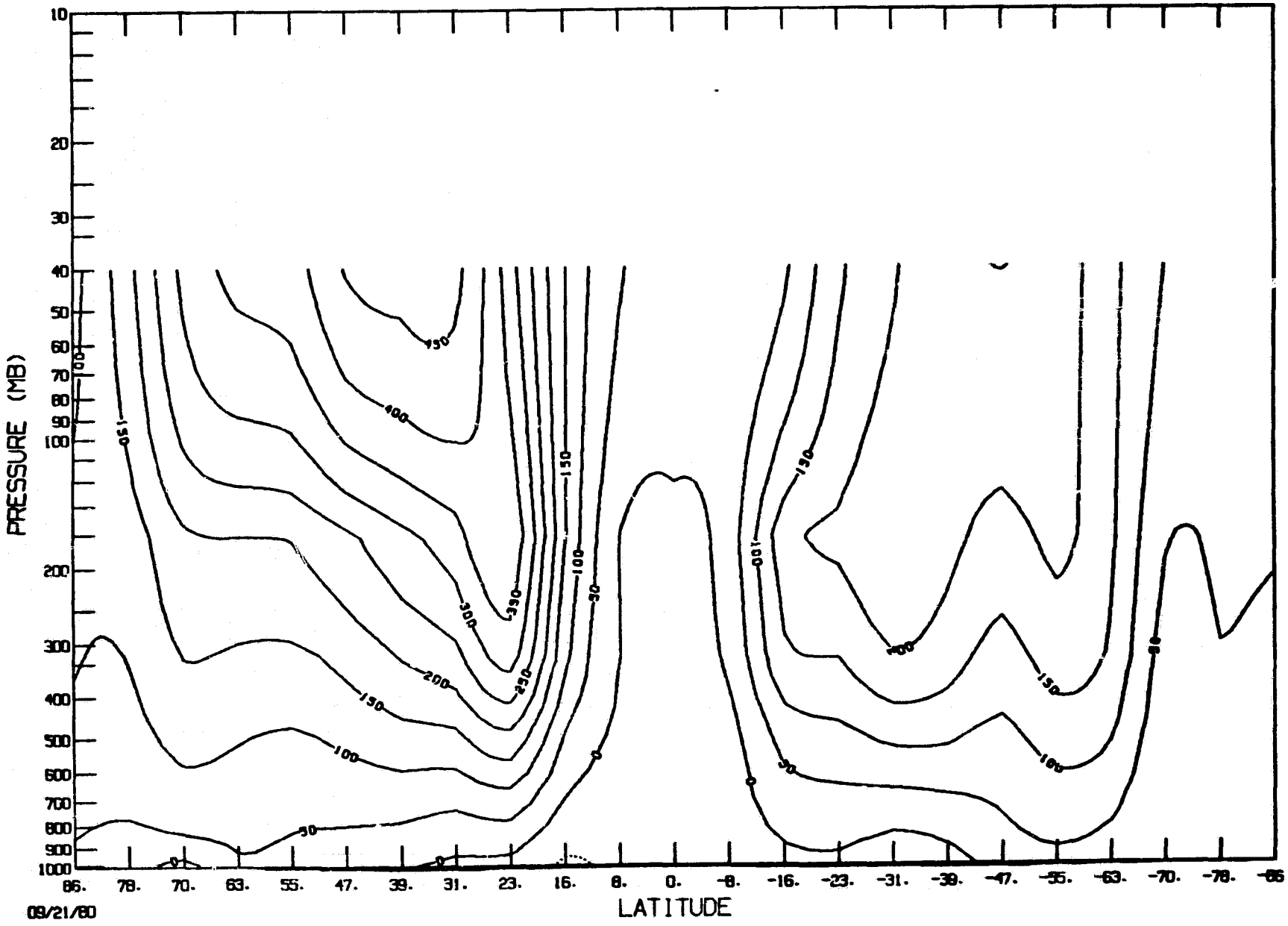

Fig. 18

a glacial advance, as illustrated in Fig. 19, where the snow line is seen to have penetrated as far south as latitude 30N over Asia and North America after 15 months. However, when the model was run for an additional 10 Januaries, the snow line not only stabilized but even retreated, at least over North America, as shown in Fig. 20 for the 20-th month. In view of the apparently non-catastrophic behavior of the continental snow cover, it was considered reasonable to average the last 18 months of the 20-January run to derive "climatological" maps (Figs. 21-23) for the flat continent experiment. (The reason for the apparent constraint on the southward spread of the snow cover is not immediately obvious, but it appears to be associated with increased warm advection associated with the development of strong thermal gradients between the fixed temperatures of the relatively warm oceans and the lowered temperatures of the snow-covered continents.)

The thermal influence of the continents appears clearly in the mean temperature map for the 1000-850 mb layer (Fig. 21), while the corresponding monsoonal sea-level pressure distribution (low pressure over the excessively heated continents of the Southern Hemisphere and high pressure over the cold continents in the Northern Hemisphere) is evident in Figure 22. The thermal effect of the continents on the 500 mb circulation can be inferred from Fig. 23. A comparison of the 18-January mean 500 mb contour pattern for the flat continent experiment with the 13-January mean for the water planet experiment (Fig. 11) shows, first of all, that the 500 mb surface is elevated over the heated continents of the Southern Hemisphere and lowered over high latitudes of the Northern Hemisphere. Otherwise, the distortion of the zonal flow by the continents is rather subtle, the most obvious effect being an east coastal trough over North America with a ridge in the North Atlantic.

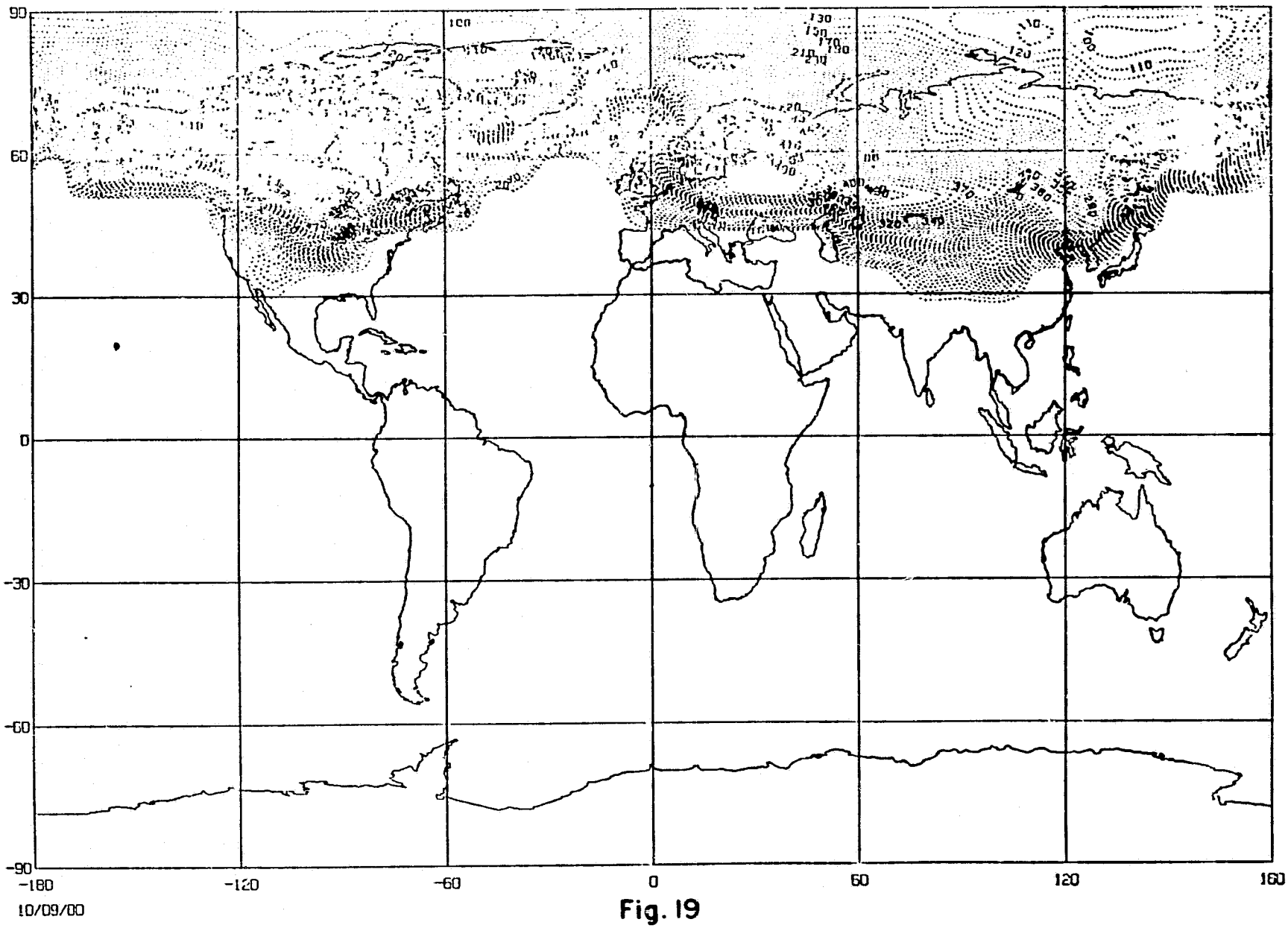

Fig. 19

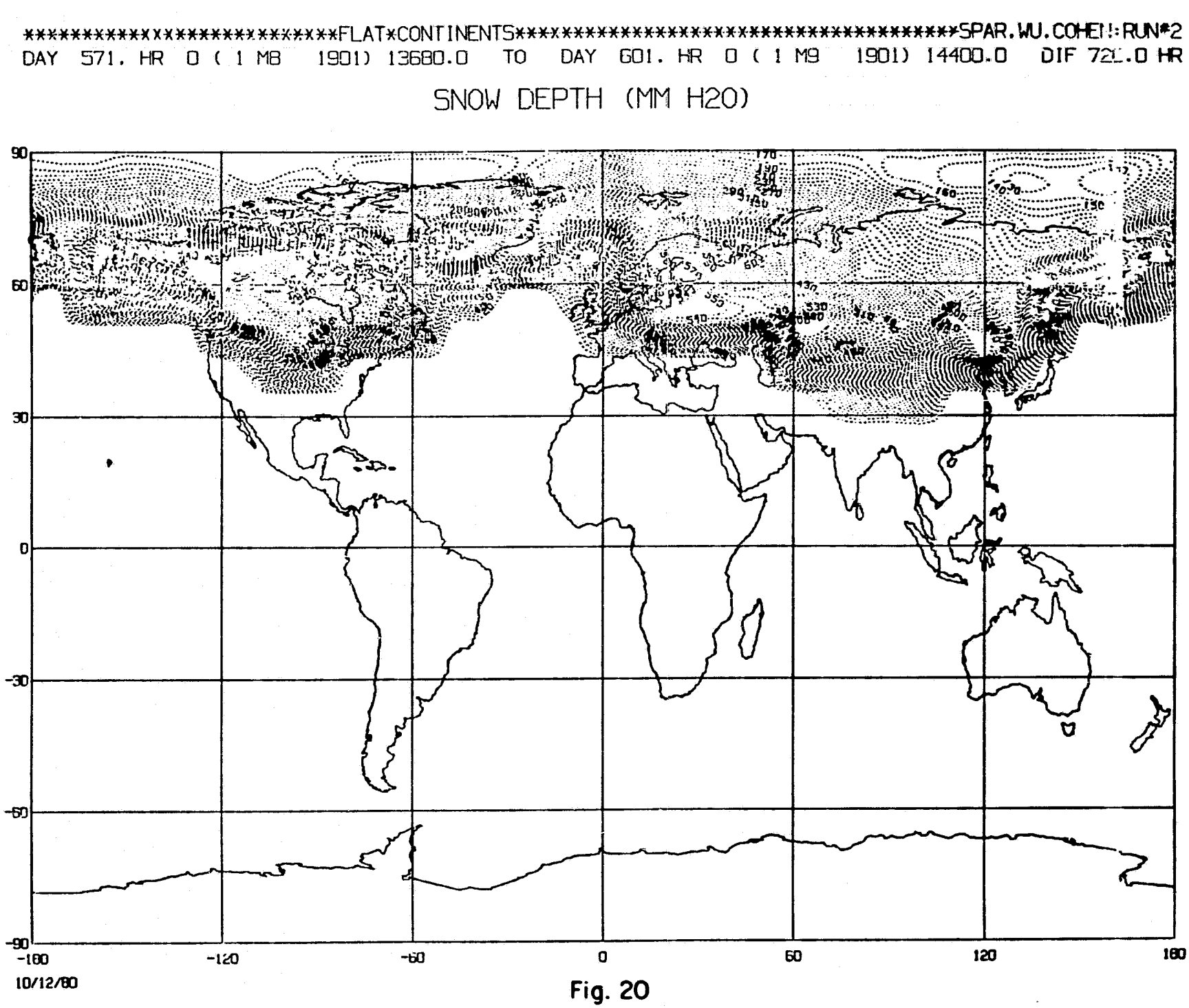
**********FLAT*CONTINENTS**********SPAR.WU.COHEN:RUN#2
DAY 571. HR 0 (1 M8 1901) 13680.0 TO DAY 601. HR 0 (1 M9 1901) 14400.0 DIF 72[illegible].0 HR
SNOW DEPTH (MM H2O)
90
60
30
0
-30
-60
-90
-180
-120
-60
0
60
120
180
10/12/80

Fig. 20

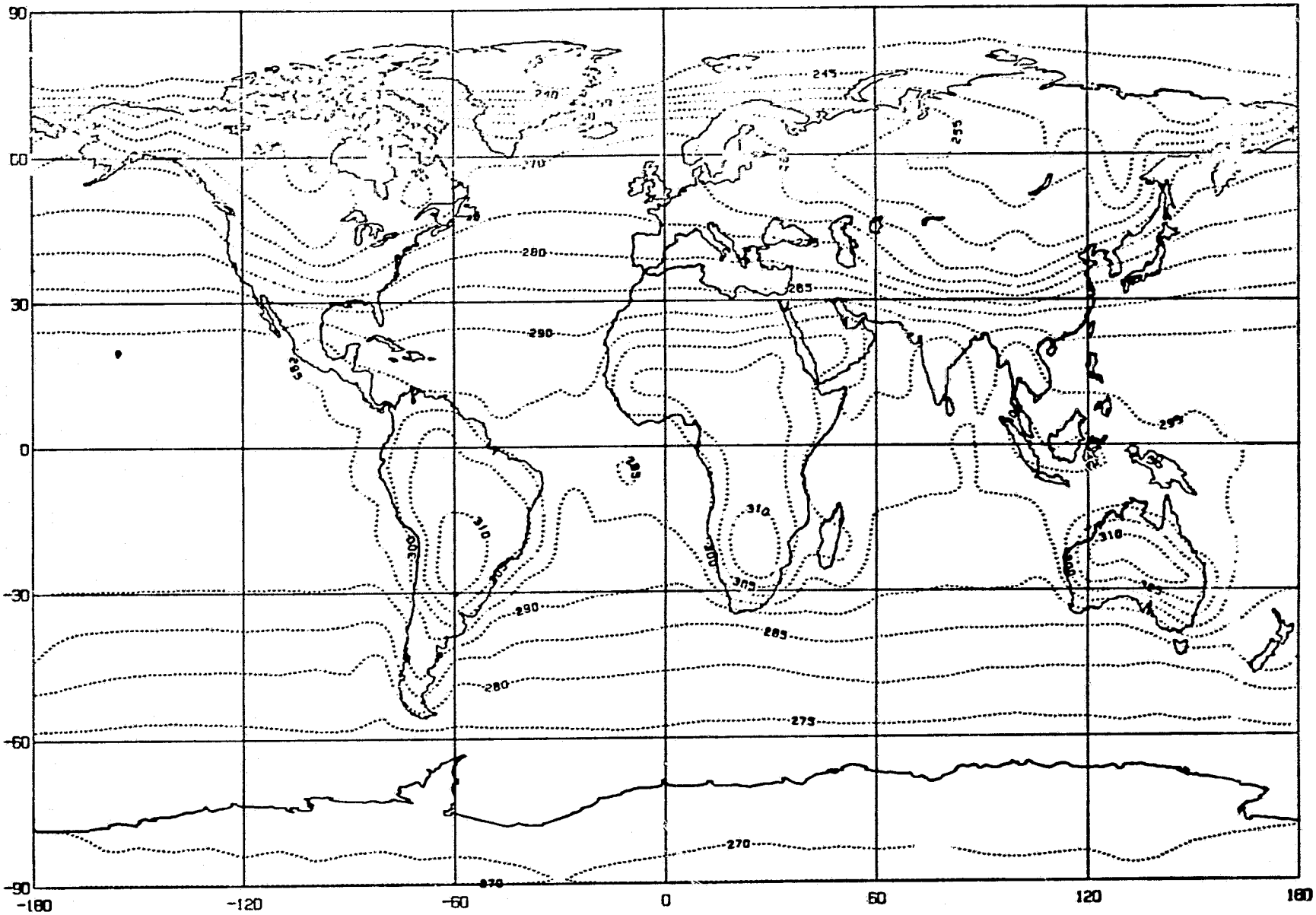

RUN002 ALL 18 MONTHS MEAN THICKNESS TEMP (1000-850MB) IN (K)

Fig. 21

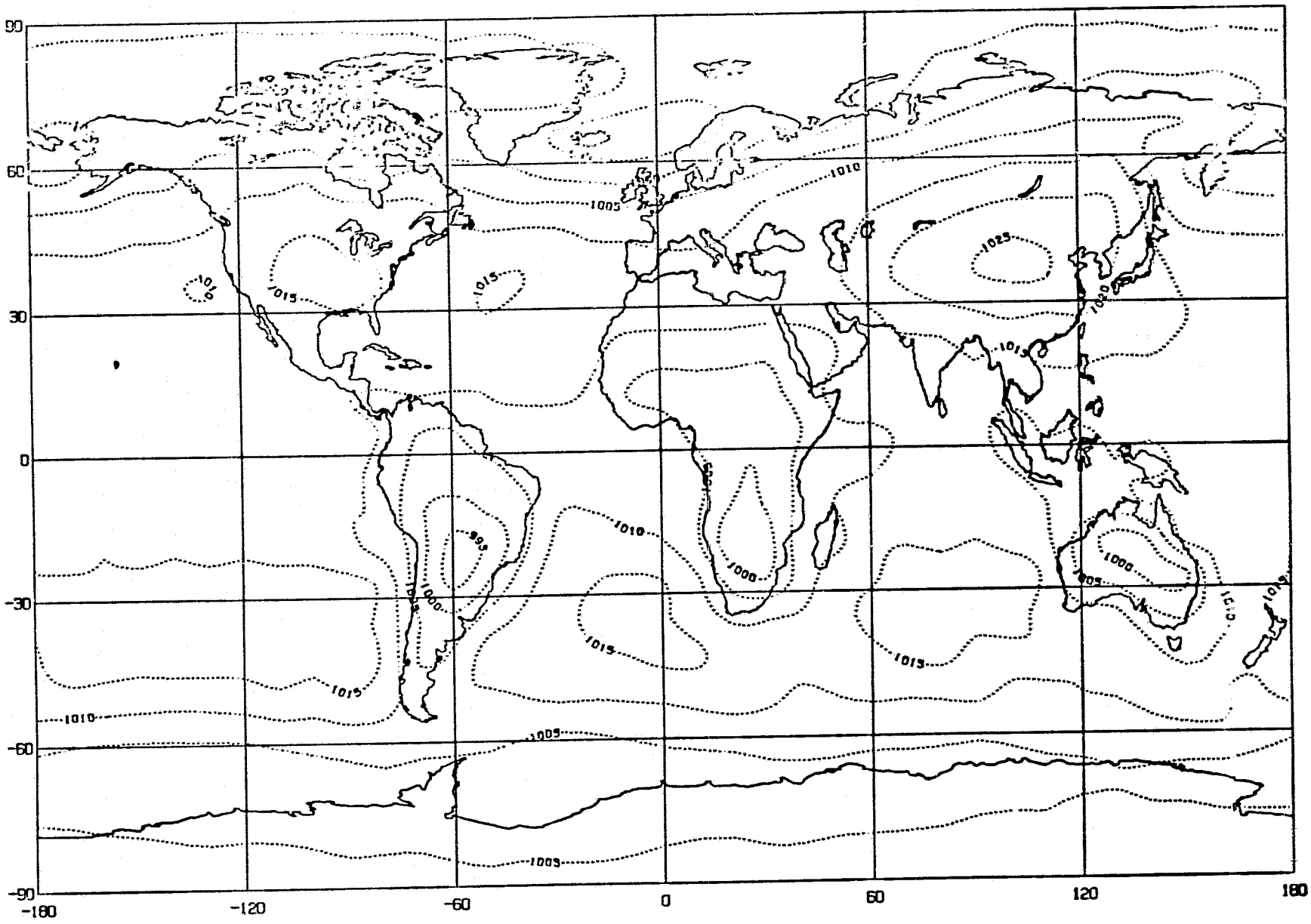

SEA LEVEL PRESSURE OF RUN002 FROM ALL 18 MONTHS MEAN (IN MB.)

Fig. 22

Fig. 23

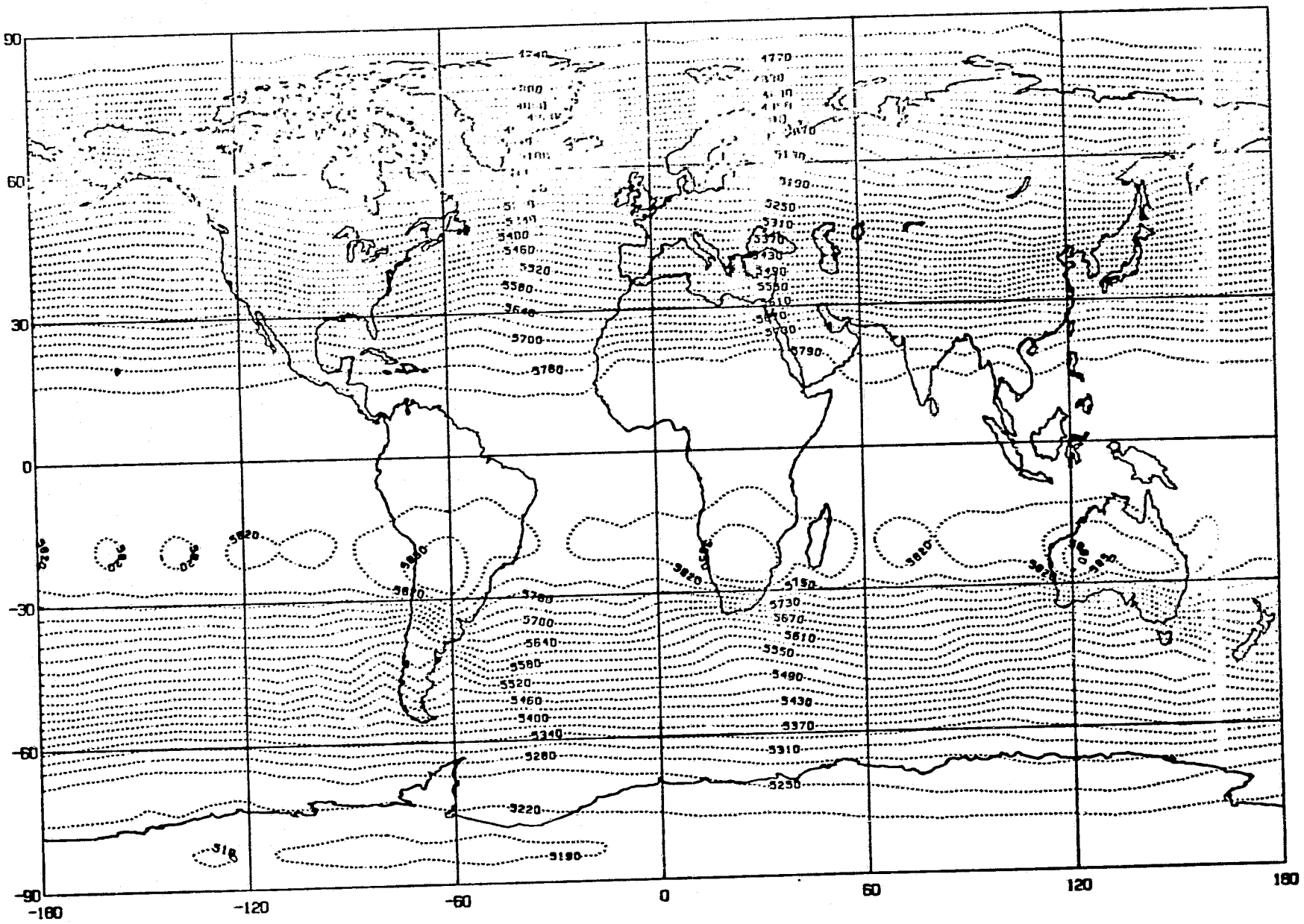

500 MB HEIGHT OFRUN002 WITH ALL 18 MONTHS MEAN (IN METERS)

Fig. 23

Compared with the observed climatological January sea-level pressure field (Fig. 24), that generated by the flat continent model (Fig. 22) exhibits certain deficiencies. The subtropical highs, the Antarctic low, and the Aleutian low[1] are all too weak, as are the associated pressure gradients, compared with the actual climatology. At the 500 mb level, the model (Fig. 23) exhibits a more zonal pattern than nature (Fig. 25), especially in the Northern Hemisphere, with stronger westerlies in the Arctic. Notably absent in the flat continent model climatology at 500 mb are the lows over the Canadian Archipelago and eastern Siberia.

(Mean maps for the flat continent experiment were also computed for the last 20 Januaries of the 25-month run, i.e. months 6 through 25, with essentially the same results, as shown in Figs. 21-23.)

The influence of the continents on the mean meridional cross-sections of temperature and zonal wind appears to be relatively small. The cross-sections for the flat continent experiment (not shown) are essentially similar to those of the water planet experiments (Figs. 12, 13, 17, 18), except for the presence of stronger equatorial easterlies.

The thermal influence of the continents may be further evaluated by comparing the global distributions of precipitation for the water planet and the flat continent model. Fig. 26 shows the daily precipitation rate for the water planet in the 10-th January, while Fig. 27 displays it for the 20-th January of the flat continent run. In the Northern Hemisphere, the continents clearly suppress precipitation in winter, while the Aleutian and Icelandic lows enhance it. Over the heated continents near the Equator and in the Southern Hemisphere precipitation is also augmented, while the oceanic precipitation in the equatorial belt is generally reduced compared with that of the water planet. The precipitation pattern over South America is quite realistic, but too much rain is computed off the coast of Peru. In the Indian and Pacific Oceans, the precipitation maxima are displaced south-

[1] A deep Aleutian low does appear after 20 Januaries, but it is located over the Bering Strait. Large inter-annual pressure fluctuations are found in this region over the 25 Januaries simulated.

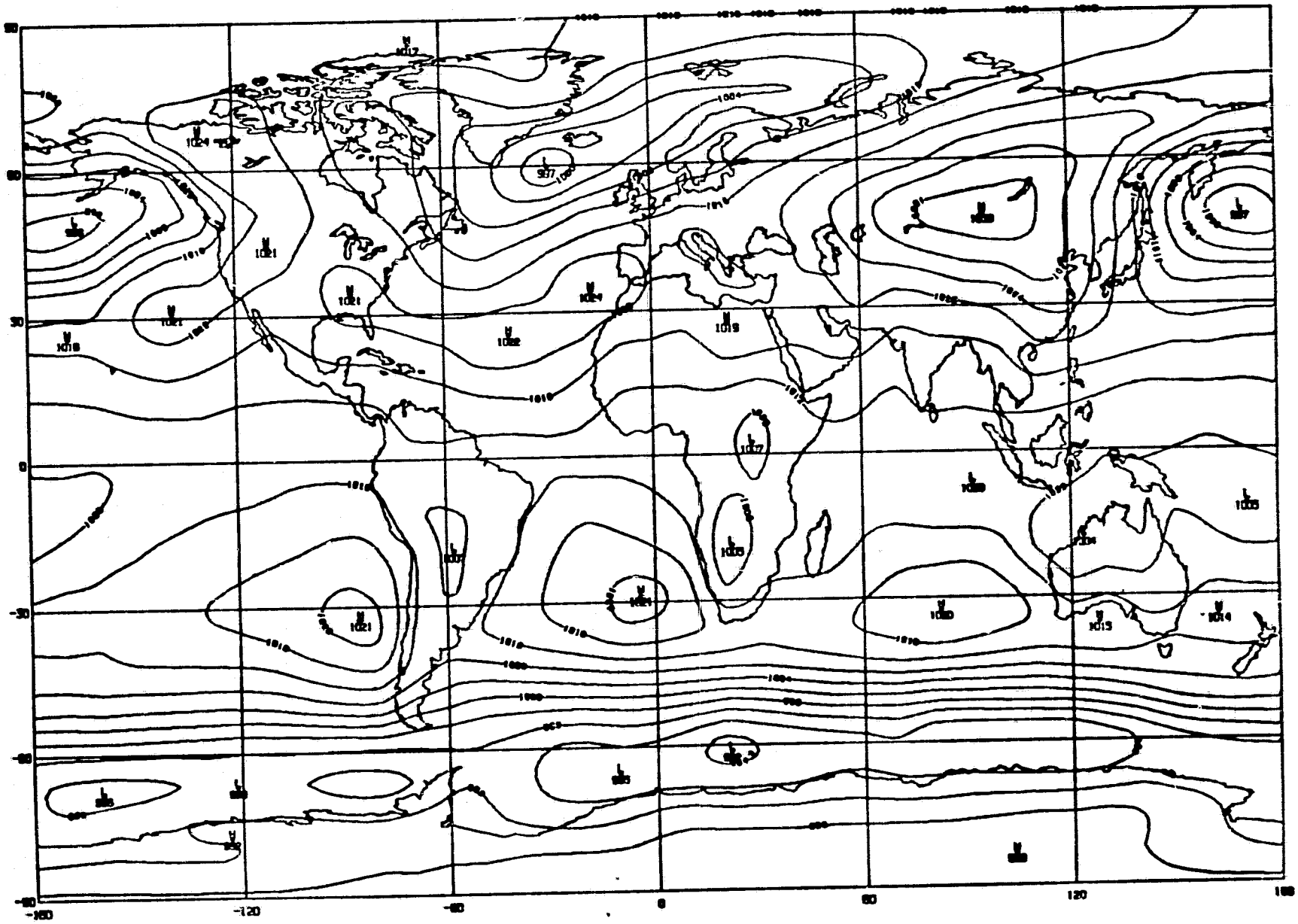

JANUARY CLIMATOLOGY SEA LEVEL PRESSURE

Fig. 24

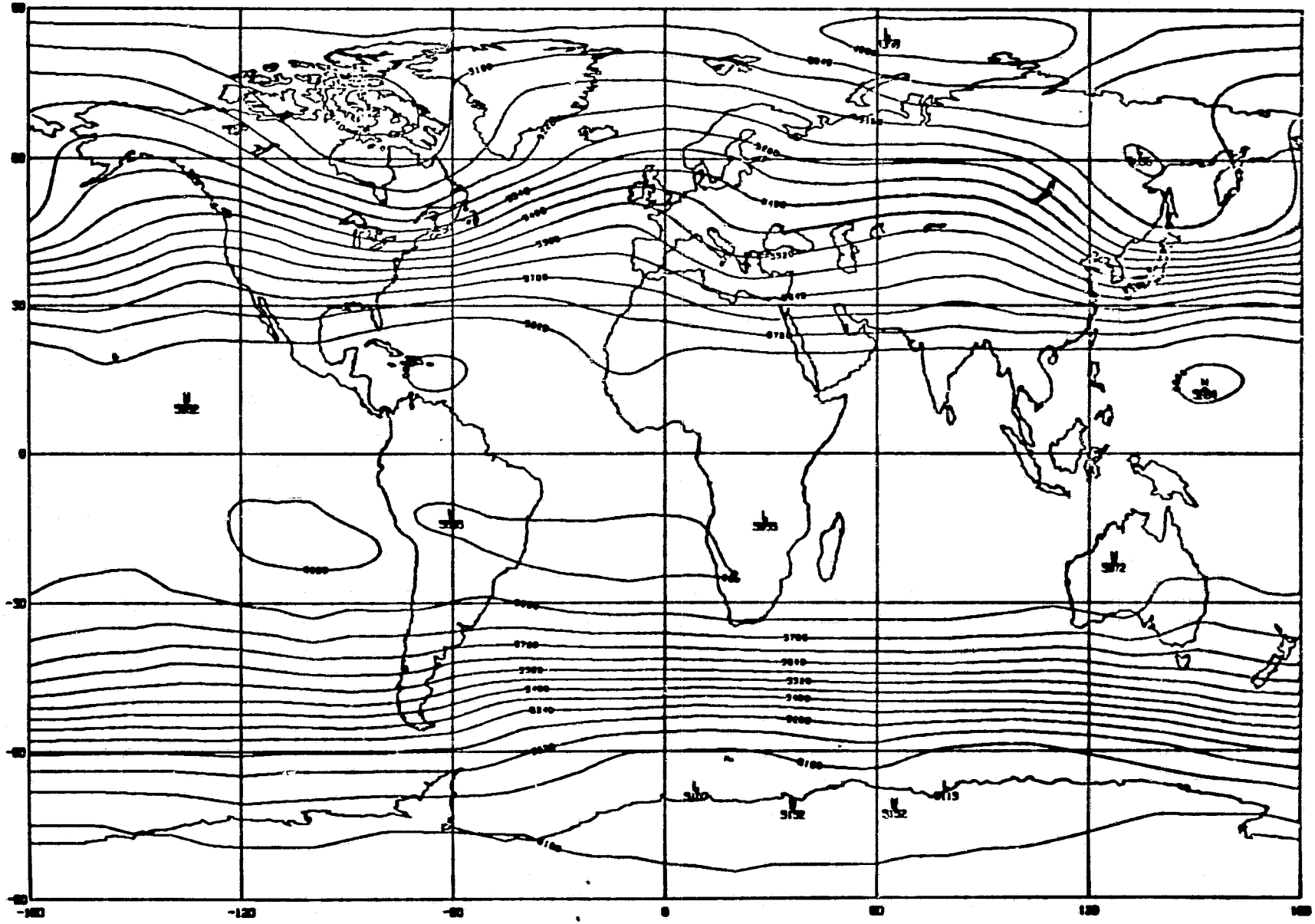

JANUARY CLIMATOLOGY 500MB GEOPOTENTIAL HEIGHT

Fig. 25

THIS IS THE OOORUN (WATER SPHERE) WITH MEAN GLOBAL TEMP . SPEC..HUMIDITY.....SPAR.COHEN.WU:RUN#O
DAY 271. HR 0 (1 M10 1900) 6480.0 TO DAY 301. HR 0 (1 M11 1900) 7200.0 DIF 720.0 HR

PRECIPITATION (MM/DAY)

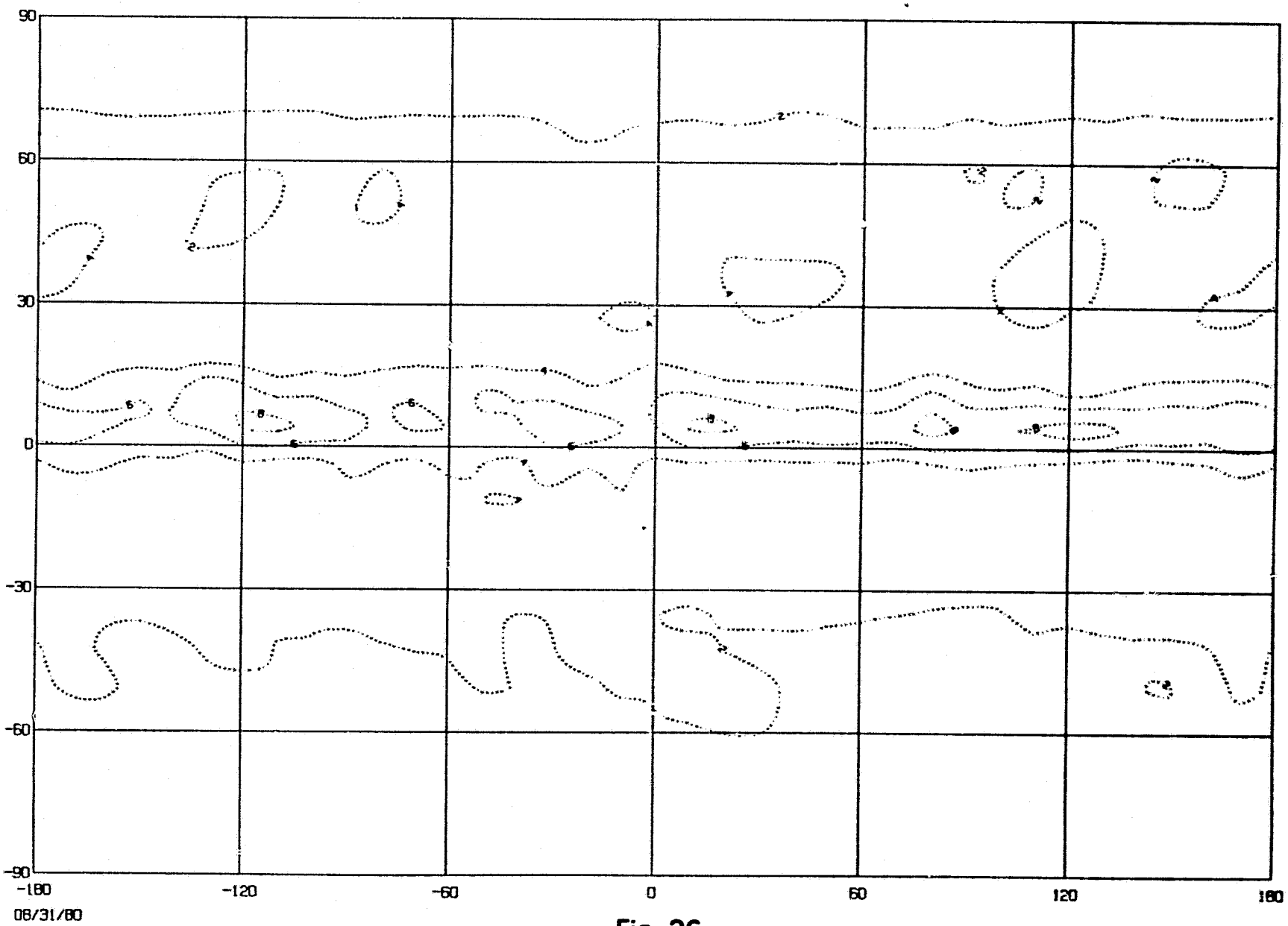

Fig. 26

**********FLAT*CONTINENTS**********SPAR.WU.COHEN:RUN#2

DAY 571. HR 0 (1 M8 1901) 13680.0 TO DAY 601. HR 0 (1 M9 1901) 14400.0 DIF 720.0 HR

PRECIPITATION (MM/DAY)

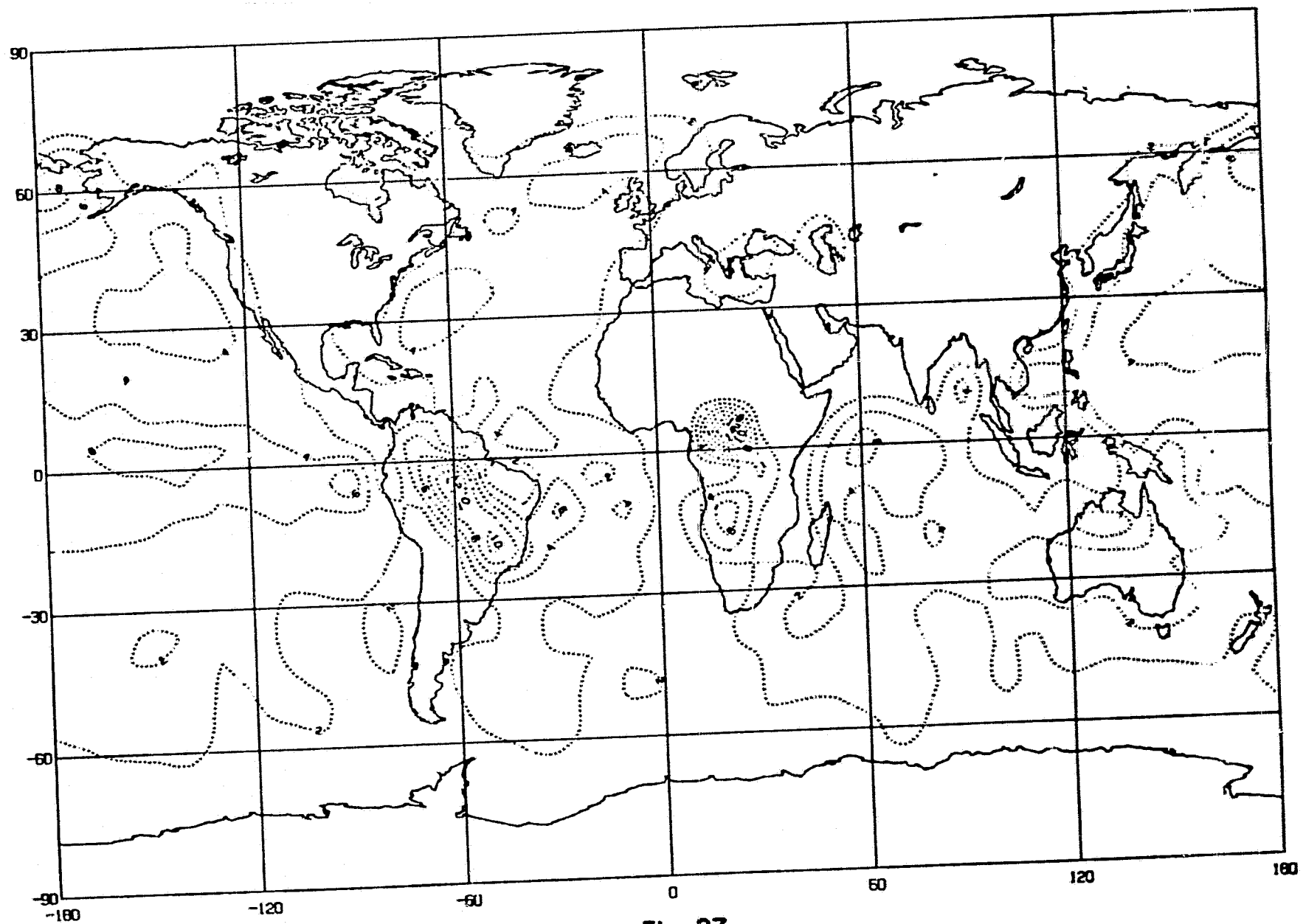

Fig. 27

ward relative to the locations of the maxima on the water planet, indicating that the continents are responsible for the southward displacement of the intertropical convergence zone in January over the oceans as well as over land. The relatively dry condition in the eastern tropical Atlantic Ocean is a particularly noteworthy (and realistic) example of the distortion of the zonally symmetric precipitation pattern by the continents.

The shift of the ITC into the Southern Hemisphere is better illustrated by the precipitation rate map for the 25-th January (Fig. 28), showing maxima south of the Equator in the Pacific and Indian Oceans. However, the dry belt on the eastern side of the tropical Pacific is again missing in the model simulation.

The role of mountains (run 003)

Both the thermal influences of the continents and the dynamic effects of mountains are known to be significant factors controlling the structure and circulation of the atmosphere. However, the relative importance and quantitative magnitude of each as a climate control is still a subject of controversy. As noted, for example, by Kasahara and Washington (1971), there is considerable evidence that, with regard to the large-scale climate, the thermal effect of continentality is far more important than that of orography, although some evidence to the contrary also exists. A comparison of the January climates generated in the "flat continent" and "mountain" experiments with the GISS coarse mesh model should provide some additional insight into this problem.

The orographic experiment differs from those preceding it not only in the inclusion of coarse mesh continental topography, but also in the use of a dry, isothermal (273 K) initial state. In this case, the model is allowed not only to spin up from a state of rest, but also to generate its own moisture field (by evaporation from the oceans), as well as vertical and horizontal temperature distributions. During the first two months of this run, the dry initial state results in extremely low radiative surface

**********FLAT*CONTINENTS**********SPAR.WU.COHEN:RUN#2
DAY 721. HR 0 (1 M1 1902) 17280.0 TO DAY 751. HR 0 (1 M2 1902) 18000.0 DIF 720.0 HR

PRECIPITATION (MM/DAY)

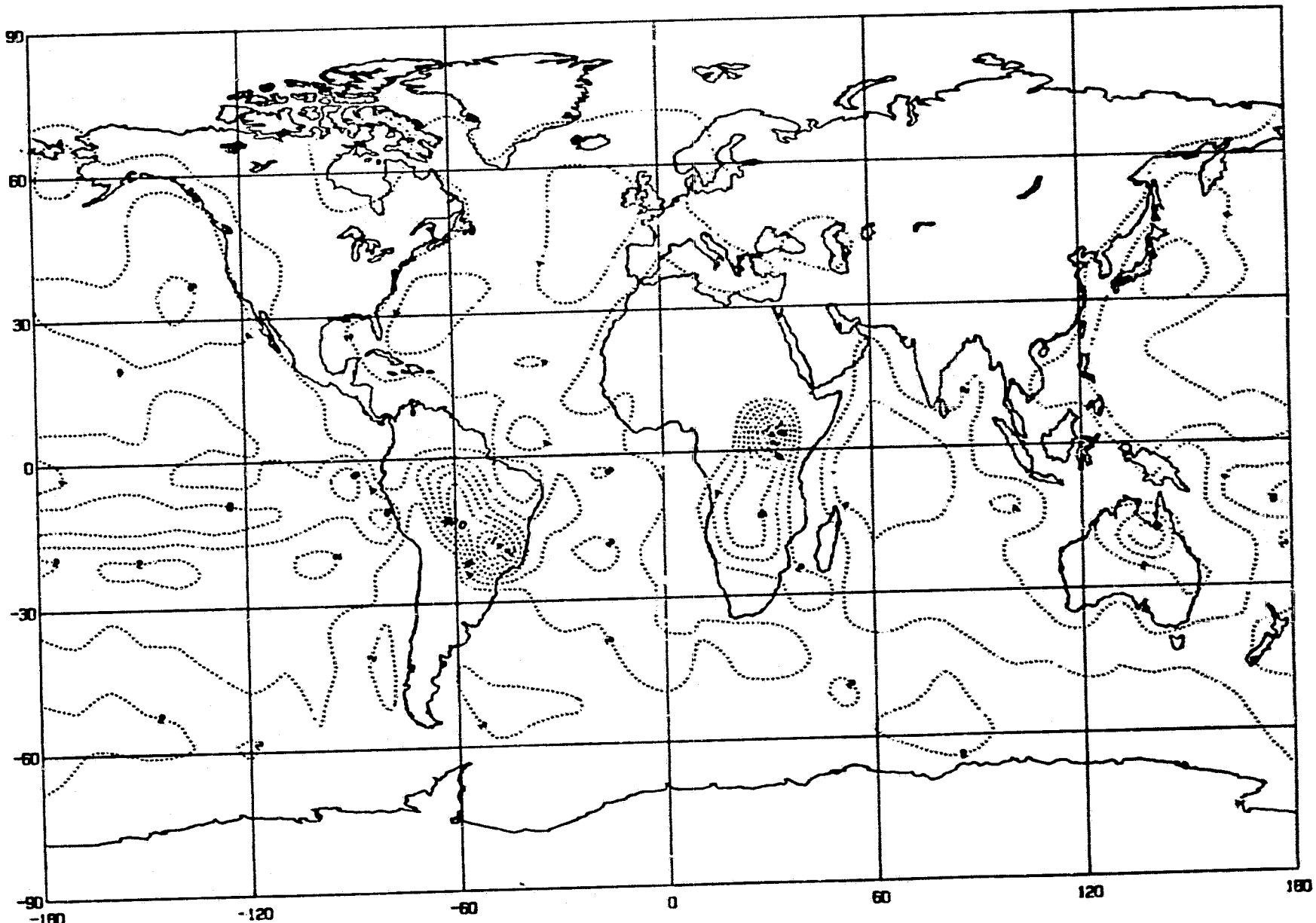

11/05/80

Fig. 28

temperatures, especially over the polar night region of the Northern Hemisphere. The cold continental conditions even produce transient snow accumulations in the subtropics. However, after several Januaries, the effects of evaporation from the sea, and the heating of the atmosphere, begin to establish realistic temperatures over most of the model atmosphere, resulting in a snow line almost identical to that of the previous (flat continent) experiment, but with lower temperatures and snow over the elevated Antarctic plateau, as shown in Fig. 29 for the 14-th January.

One source of difficulty in the mountain experiment is Greenland, where the elevated glacier generates extremely low temperatures and, hence, excessively high sea-level pressures due to the method of reducing station pressures to sea level. On the other hand, the snow-covered Antarctic plateau produces more realistic surface temperatures on that glacier in the January mountain experiment than in the flat continent run, as shown in Fig. 30 for the 14-th January.

Because of the dry initial state in the mountain experiment, the model was run for 25 Januaries, and the first 5 months were discarded as transients before averaging. The resulting 20-January mean maps may then be compared with the corresponding mean maps for the flat continent run.

The 20-January (6-25) mean maps of precipitation rate for the "flat continent" run (002) and the "mountain" run (003) are shown in Figs. 31 and 32, respectively. A comparison of the two fields indicates only small effects of the coarse mesh mountains on the precipitation in the Northern (winter) Hemisphere. Relatively modest increases are seen in the region of the Appalachian Mountains (south of the Great Lakes) and on the west coast of North America. However, much larger differences are found over the warm, moist regions of Africa and South America, with greater precipitation indicated in the mountain run, not only where the terrain would account for it (e.g., in the Andes and over the south African highlands), but also where there should be

*****RUN003*SPIN UP WITH ISOTHERMAL ATMOSPHERE INCLUDING MOUNTIAN*ZERO GROUND WETNESS SPAR.COHEN.W
DAY 391. HR 0 (1 M2 1901) 9360.0 TO DAY 421. HR 0 (1 M3 1901) 10080.0 DIF 720.0 HR

SNOW DEPTH (MM H2O)

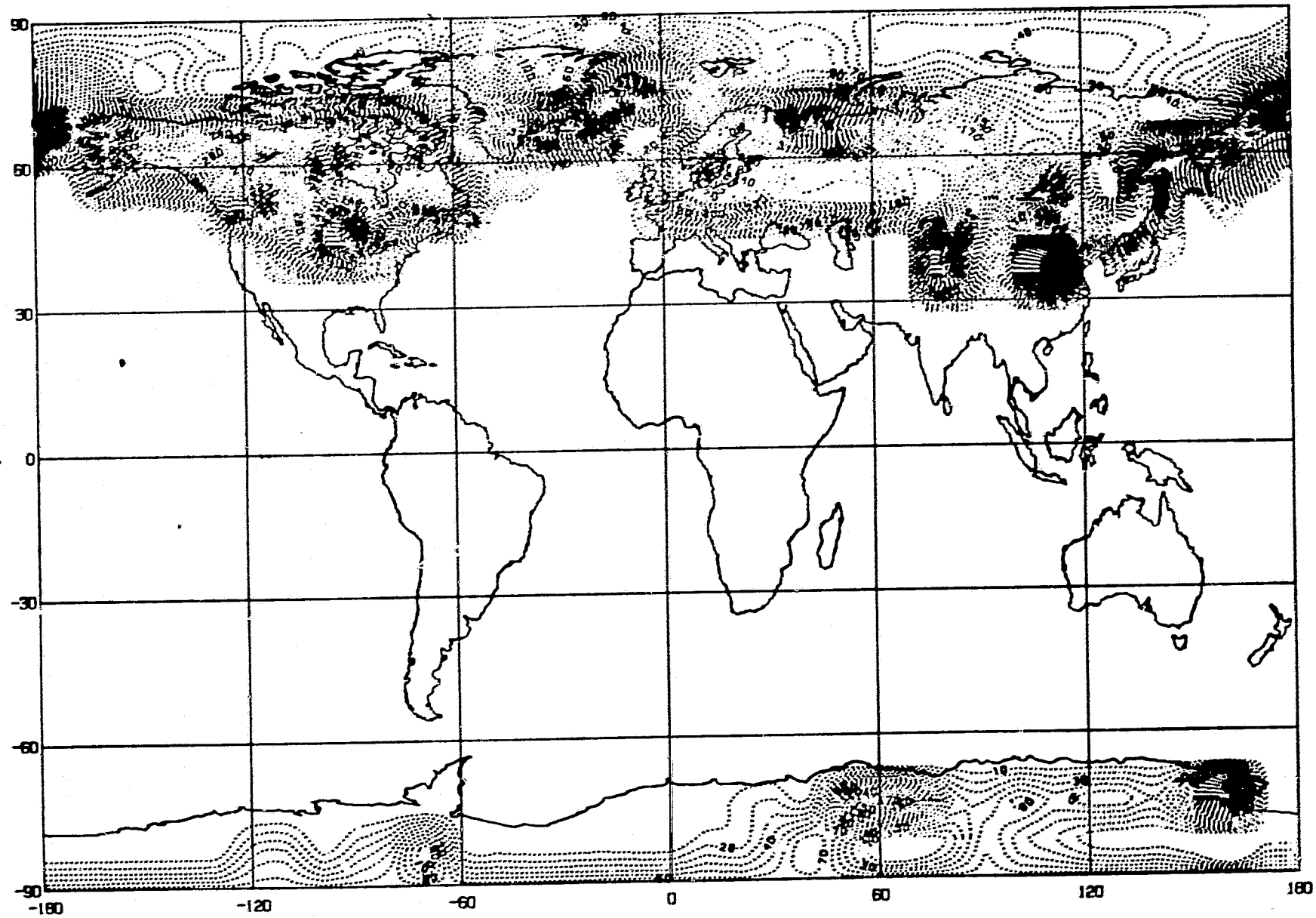

11/12/80

Fig. 29

*****RUN003*SPIN UP WITH ISOTHERMAL ATMOSPHERE INCLUDING MOUNTIAN*ZERO GROUND WETNESS SPAR.COHEN.W
DAY 391. HR 0 (1 M2 1901) 9360.0 TO DAY 421. HR 0 (1 M3 1901) 10080.0 DIF 720.0 HR

SURFACE TEMPERATURE (DEG C)

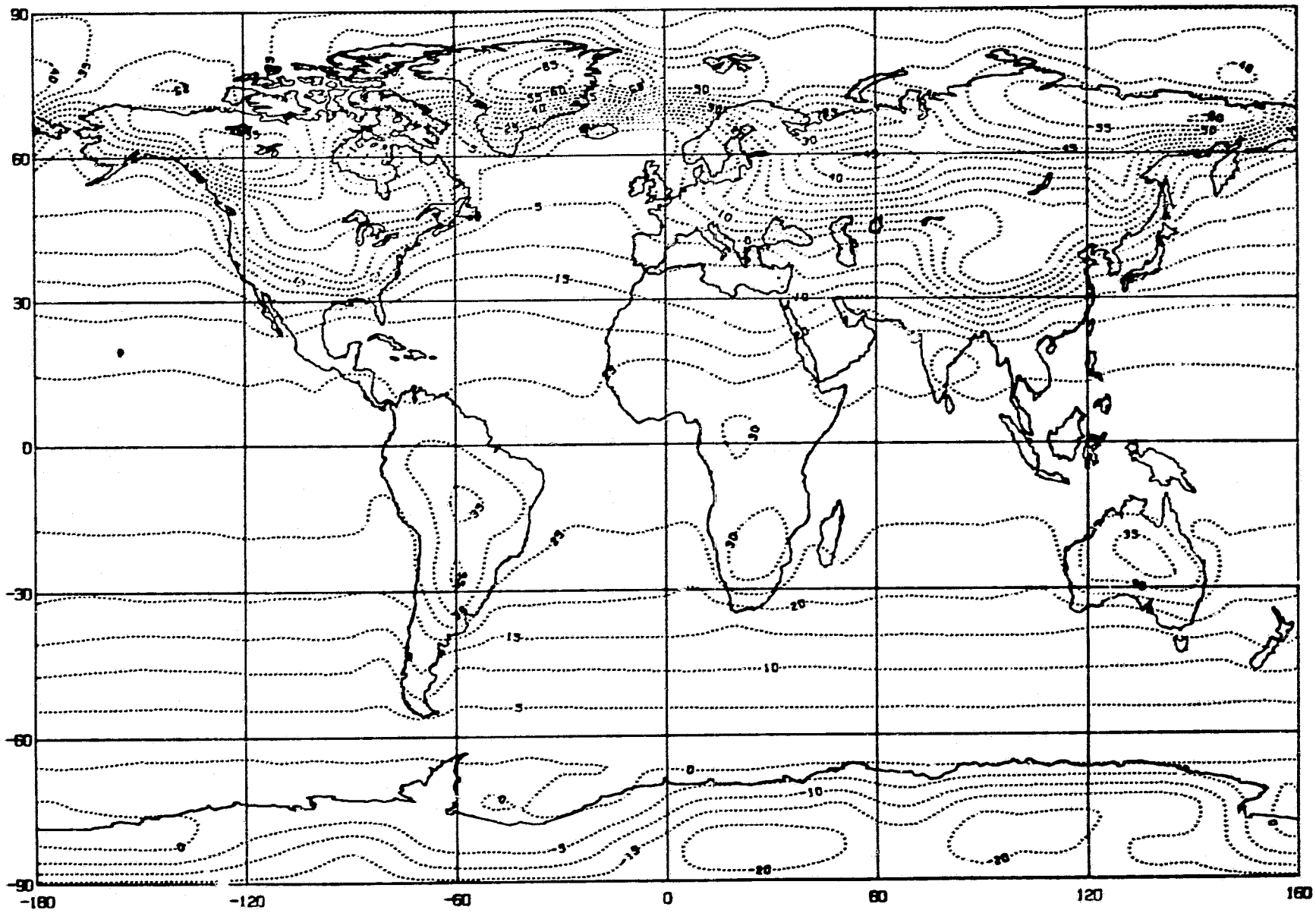

11/12/80

Fig. 30

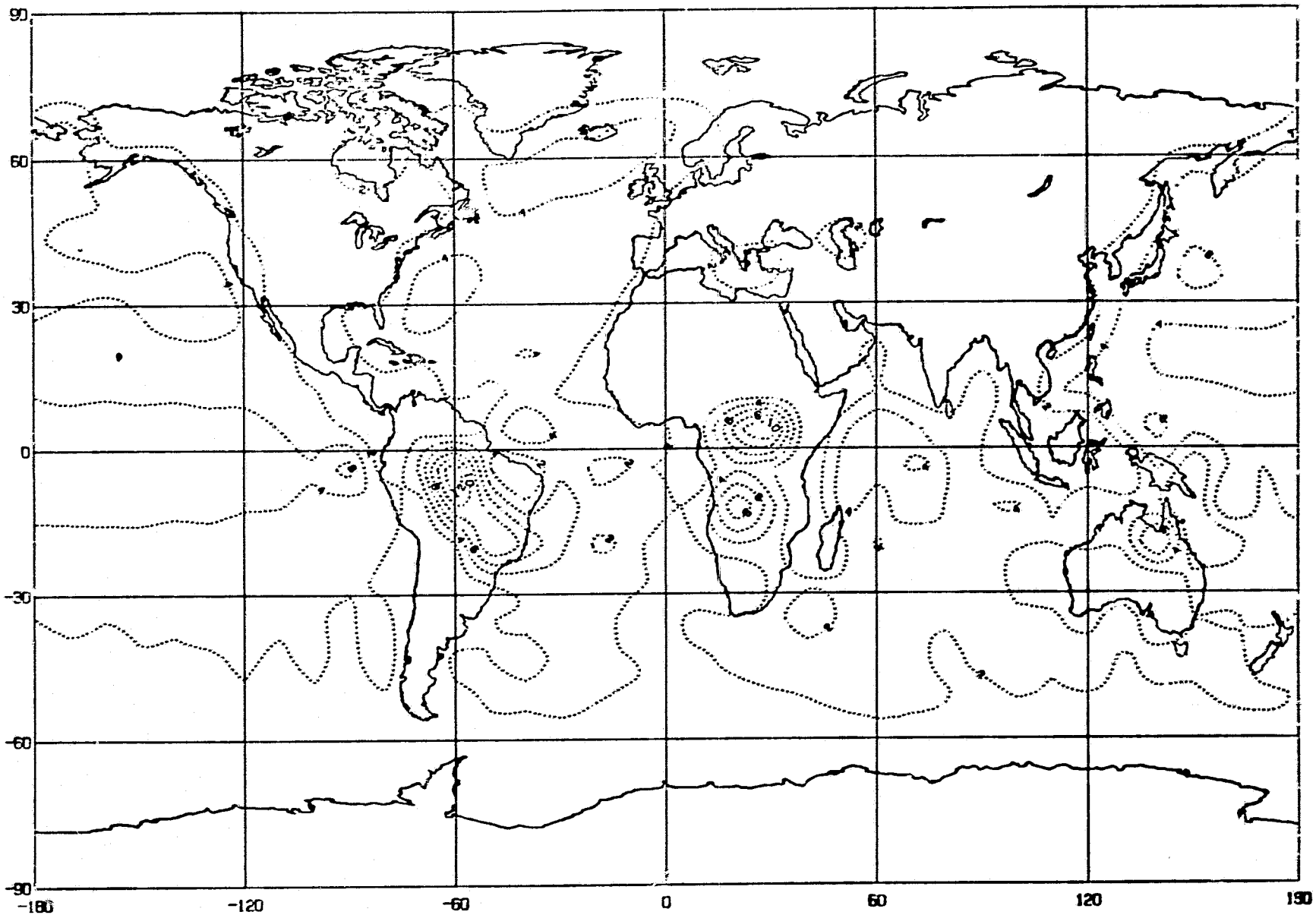

PRECIPITATION OF LAST 20MONTHS MEAN IN.(MM/DAY)SPIN UP RUN002

FIG. 31

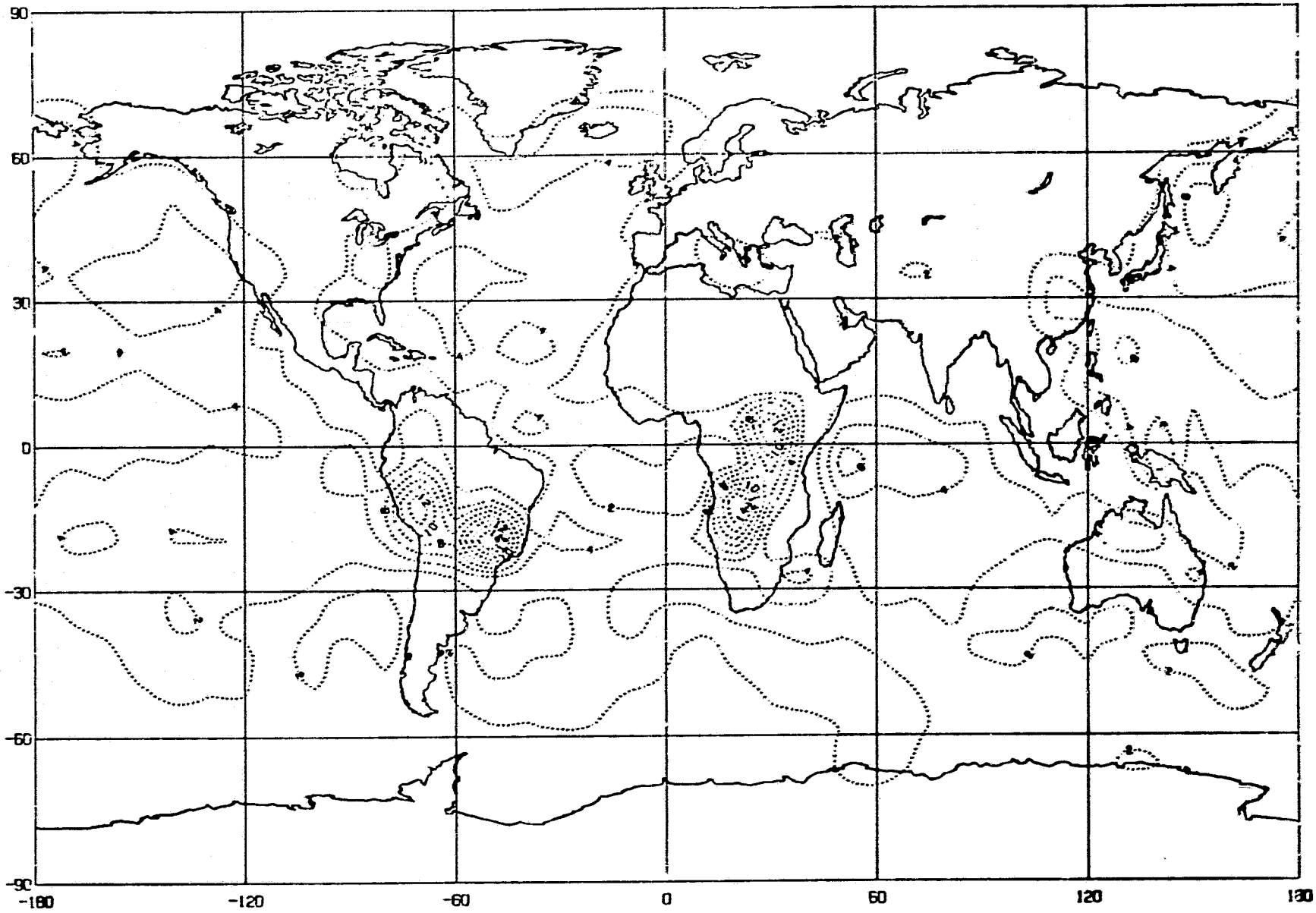

PRECIPITATION OF LAST 20MONTHS MEAN IN (MM/DAY) SPIN UP RUN003

FIG. 32

no orographic component (e.g., eastern South America). Indeed, the change in the orientation and intensity of the precipitation pattern over South America appears to be one of the major consequences of the addition of mountains.

The mean surface temperatures for the last 20 Januaries (6-25), shown in Figures 33 and 34 for the flat continent and mountain runs, respectively, exhibit not only the expected effects of altitude on temperature (see, e.g., the Atlantic, Greenland, the Tibetan plateau, and southern Africa), but also some residual low temperatures apparently resulting from the dry initialization of the mountain run (see, e.g., northeastern Siberia).

Mean meridional cross-sections of zonal winds for the last three experiments (Figs. 35-37) illustrate some of the effects of the continents and the mountains on the zonal circulation of the model atmosphere. Fig. 35 is for the water planet run, Fig. 36 for the flat continent run, and Fig. 37 for the mountain run. The principal differences between the water planet and flat continent cross-sections are found in the equatorial easterlies (stronger with continents) and in the horizontal wind shear in the subtropics of the Southern Hemisphere (stronger with continents). The effect of mountains, as illustrated by the difference between Figs. 36 and 37 is clearly smaller than that of the continents.

(As the experiment is still incomplete, no attempt will be made at this time to summarize results or to draw premature conclusions.)

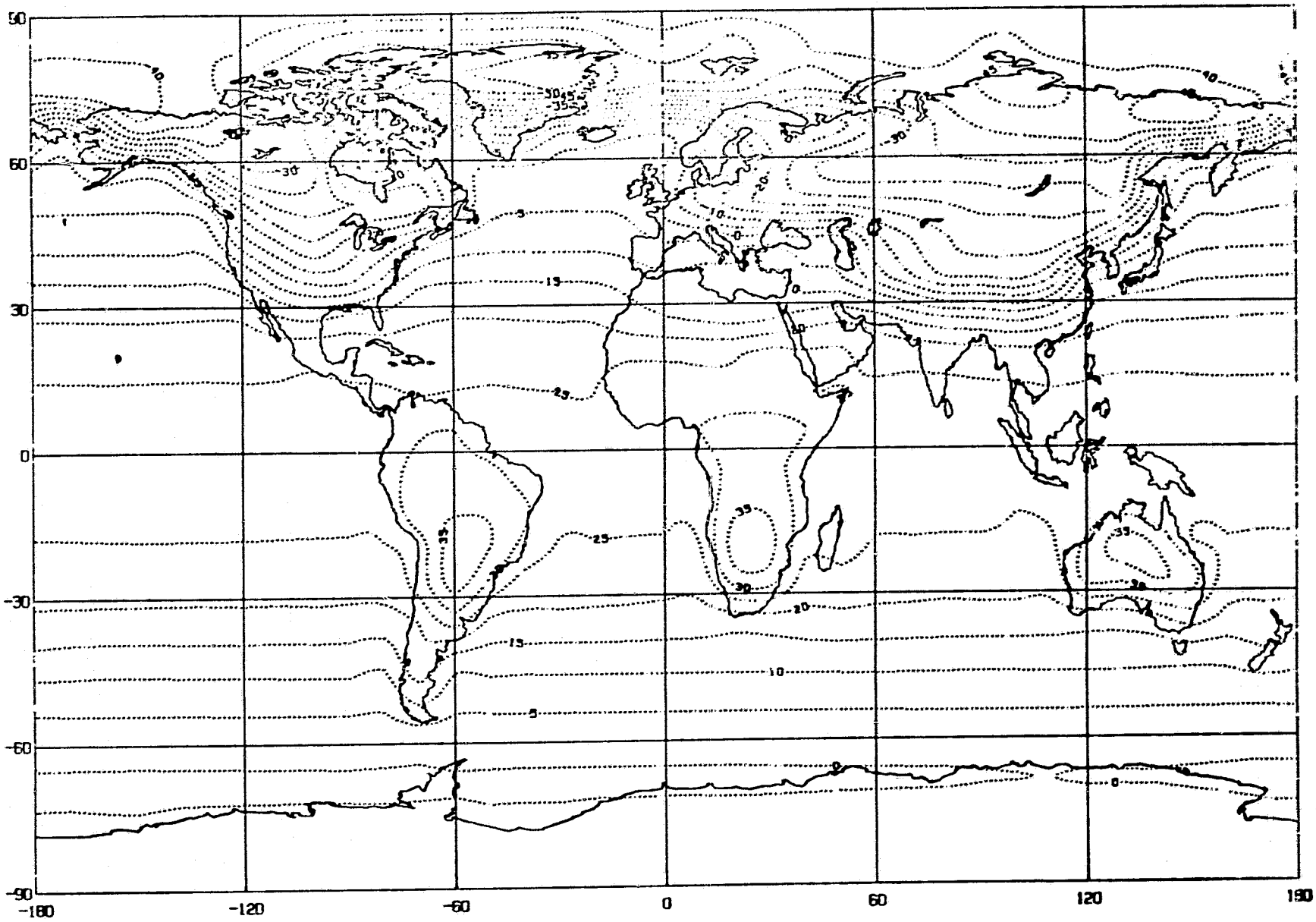

SURFACE TEMPERATURE OF RUN 002 THE AVERAGE OF LAST 20 MONTHS

FIG. 33

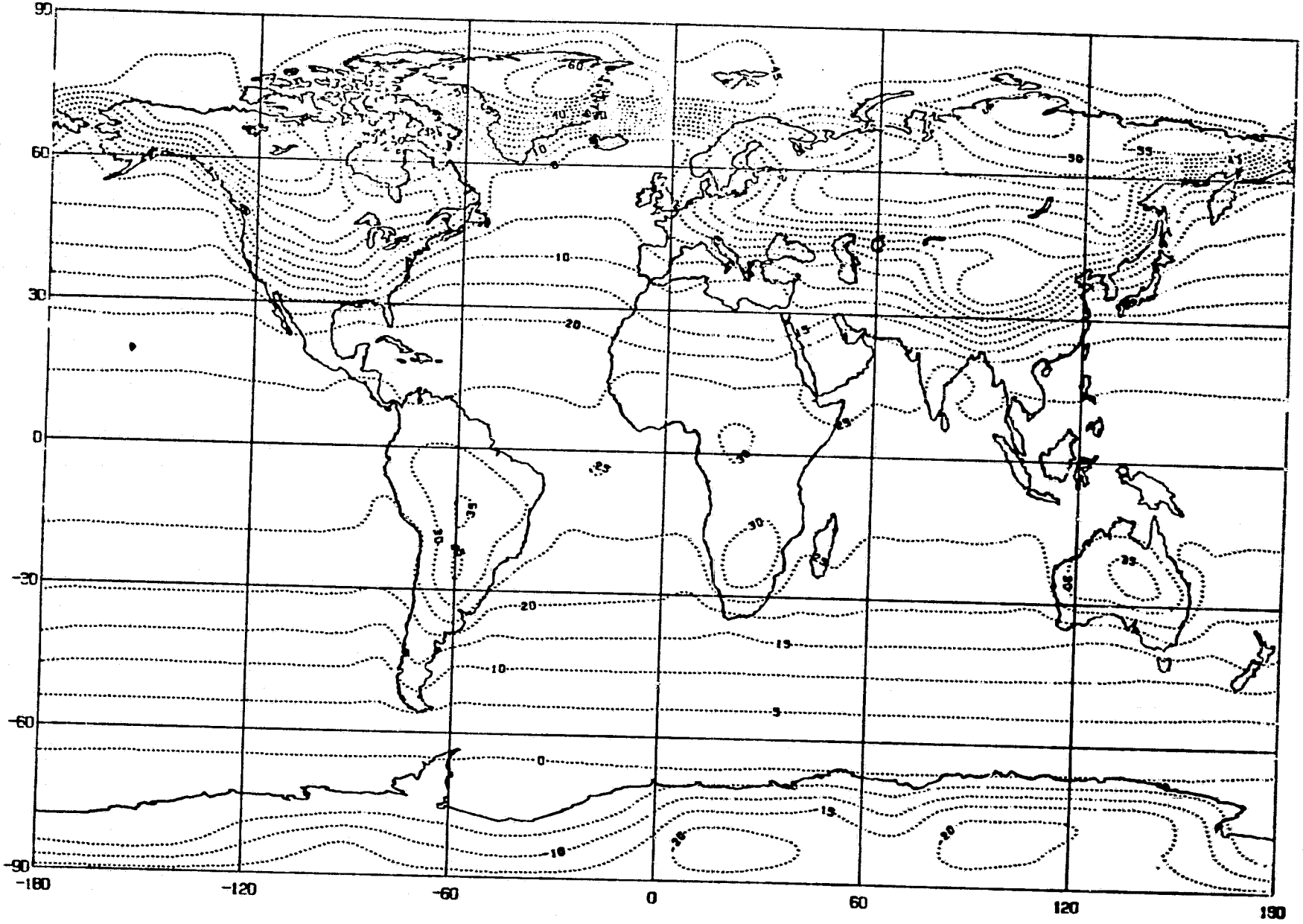

SURFACE TEMPERATURE OF RUN 003 THE AVERAGE OF LAST 20 MONTHS

FIG. 34

THIS IS THE OOORUN (WATER SPHERE) WITH MEAN GLOBAL TEMP . SPEC..HUMIDITY.....SPAR.COHEN.WU:RUN#O

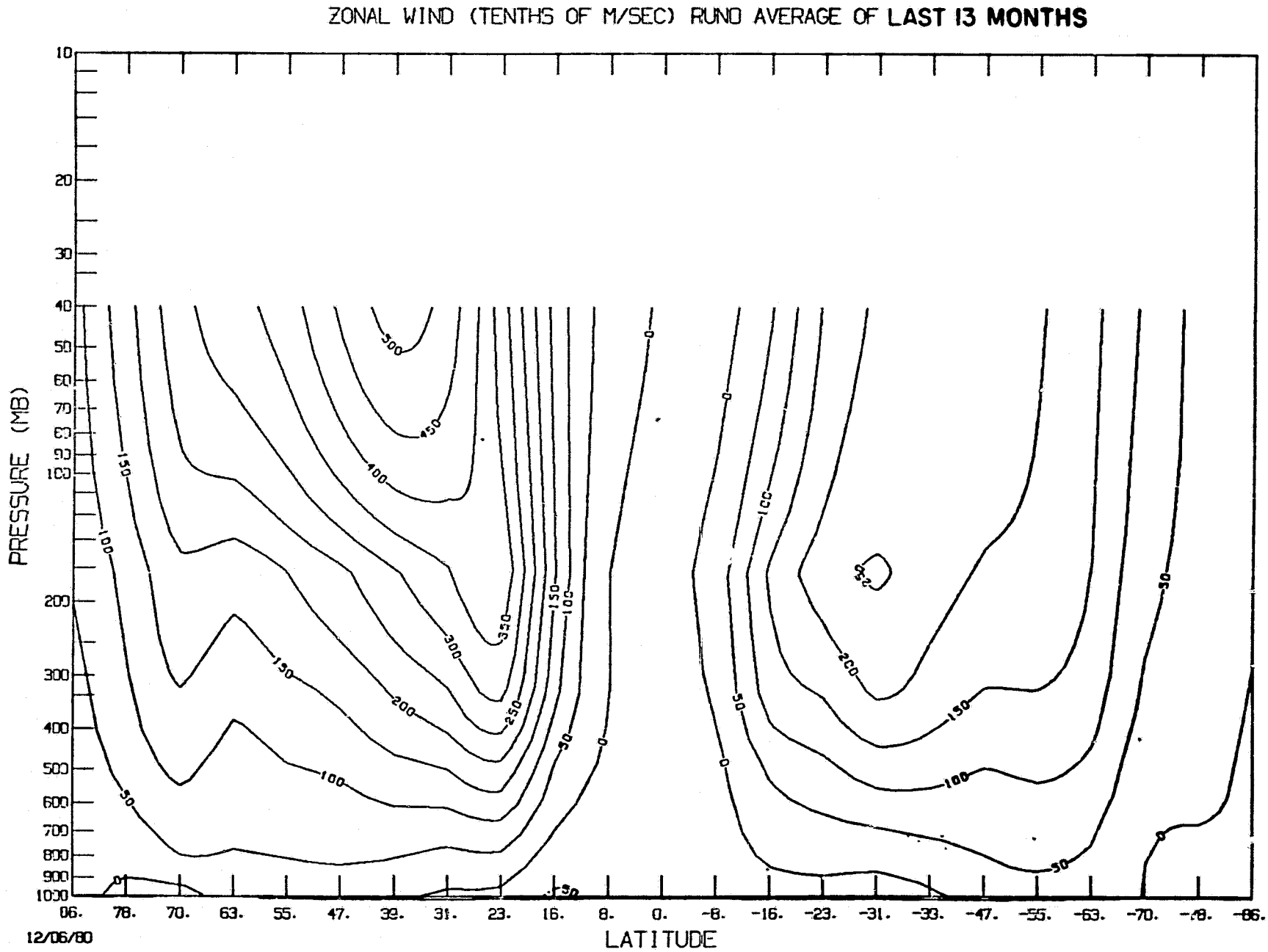

FIG. 35

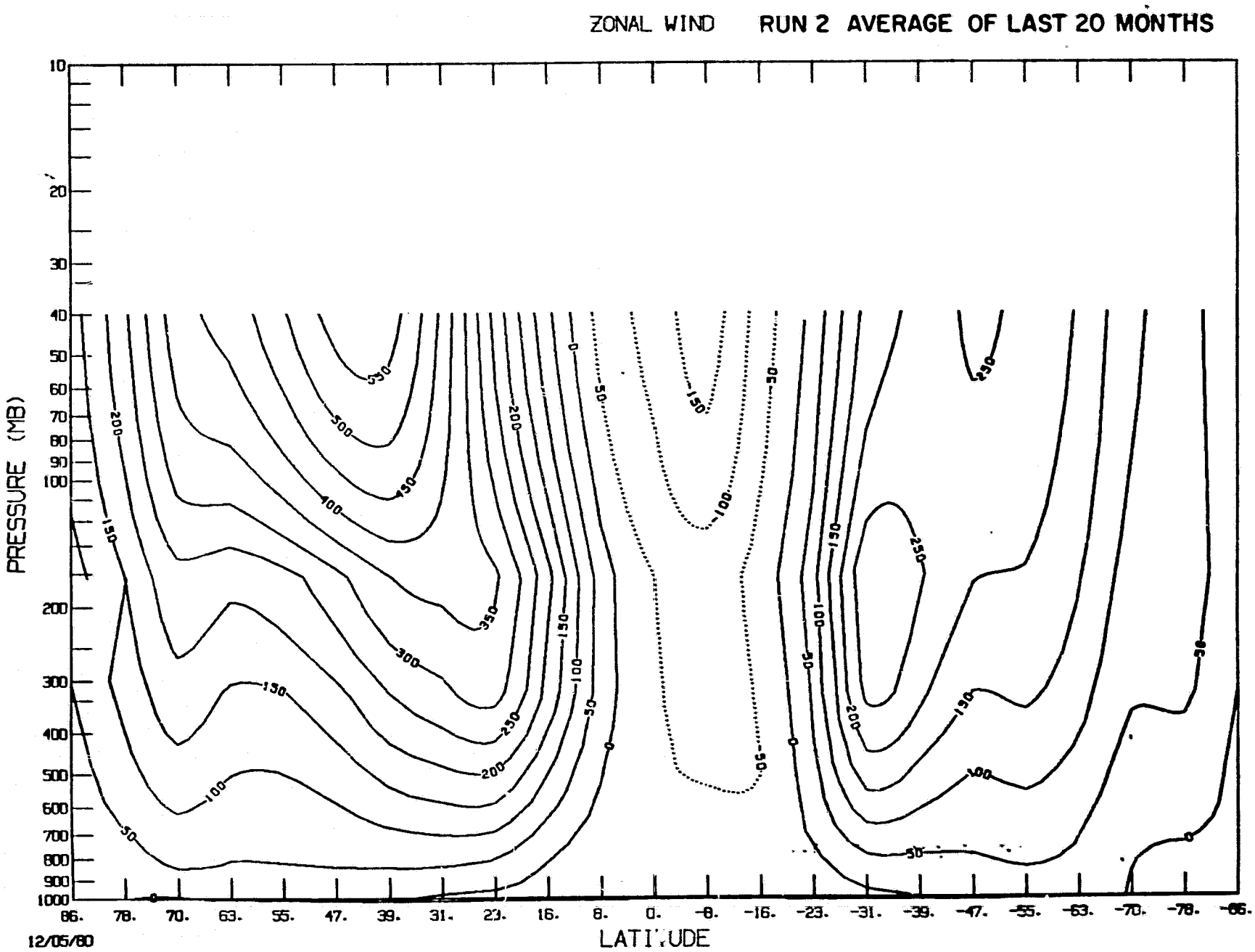
ZONAL WIND RUN 2 AVERAGE OF LAST 20 MONTHS
PRESSURE (MB)
10
20
30
40
50
60
70
80
90
100
200
300
400
500
600
700
800
900
1000
86. 78. 70. 63. 55. 47. 39. 31. 23. 16. 8. 0. -8. -16. -23. -31. -39. -47. -55. -63. -70. -78. -86.
LATITUDE
12/05/80

FIG. 36

*****RUN003*SPIN UP WITH ISOTHERMAL ATMOSPHERE INCLUDING MOUNTIAN*ZERO GROUND WETNESS SPAR.COHEN.W

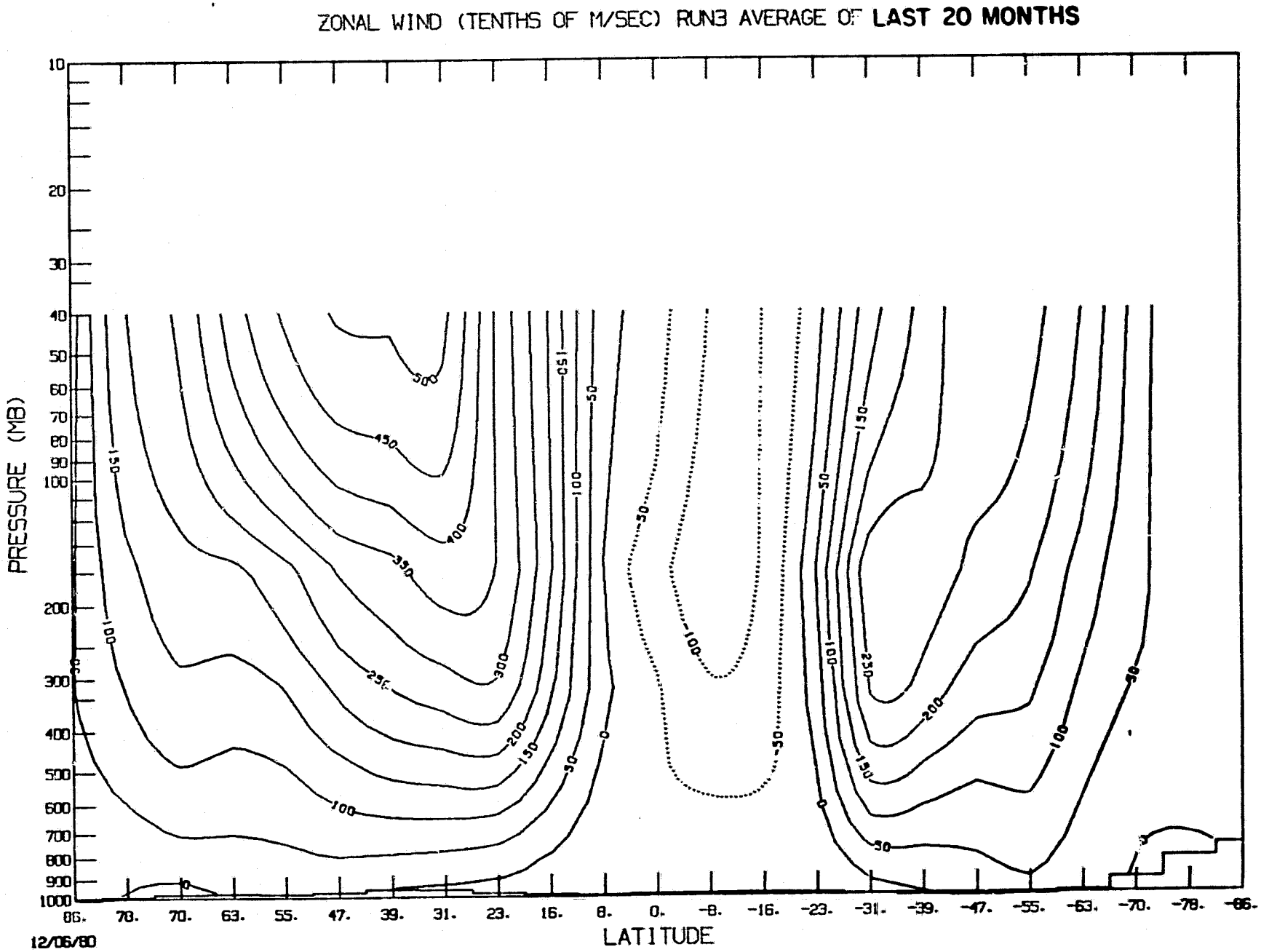

FIG. 37

References

Hansen, J., G. Russell, D. Rind, P. Stone, A Lacis, L. Travis, S. Lebedeff, and R. Ruedy, 1980: An efficient three-dimensional global model for climate studies. I. Model I. NASA, Goddard Institute for Space Studies, Goddard Space Flight Center, N.Y., N.Y. 10025

Christidis, Z. D. and J. Spar, 1980: Spherical harmonic analysis of a model-generated climatology. (To be published in the Monthly Weather Review, February 1981).

Kasahara, A. and W. M. Washington, 1971: General circulation experiments with a six-layer NCAR model, including orography, cloudiness and surface temperature calcuations. J. Atmos Sci., 27, 1122-1137.

Figures

1. Mean January surface pressure (mb) vs. latitude for 13 months (3-15) of model run 001 (water planet, with zonal mean initial conditions).

2. Mean January vertically-averaged zonal wind (ms^{-1}) vs. latitude for model run 001. Initial state, dashed; 13-month (3-15) average, solid.

3. Mean January meridional wind component ($cm\ s^{-1}$) vs. latitude in the lowest layer of the climate model, run 001. Initial state, dashed; 13-month (3-15) average, solid.

4. Mean vertically-averaged January vertical velocity ($mm\ s^{-1}$) vs. latitude for 13 months (3-15) of model run 001.

5. Vertical profiles of mean January zonal winds (ms^{-1}) vs. pressure at latitudes 39N and 37S for model run 001. Initial state, dashed; 13-month (3-15) average, solid.

6. Mean January sea-level pressure field (mb) for month No. 3 from model run 001.

7. Mean January sea-level pressure field (mb) for 13 months (3-15) of model run 001.

8. Mean January temperature (K) of layer 1000-850 mb for 13 months (3-15) of model run 001.

9. Mean January temperature (K) of layer 700-500 mb for 13 months (3-15) of model run 001.

10. Mean January geopotential height (m) of 700 mb level for 13 months (3-15) of model run 001.

11. Mean January geopotential height (m) of 500 mb level for 13 months (3-15) of model run 001.

12. Mean meridional cross-section of temperature (^{o}C) for 15-th January of model run 001.

13. Mean meridional cross-section of zonal wind ($10^{-1}\ ms^{-1}$) for 15-th January of model run 001.

14. Mean January sea-level pressure field (mb) for first month of model run 000 (water planet spin-up experiment).

Figures (Cont'd.)

15. Evolution of mean January surface pressure profile (mb) vs. latitude during first 3 months of model run 000.

16. Mean January sea-level pressure field (mb) for 13 months (3-15) of model run 000.

17. Mean meridional cross-section of temperature (^{o}C) for 15-th January of model run 000.

18. Mean meridional cross-section of zonal wind (10^{-1} ms^{-1}) for 15-th January of model run 000.

19. January snow cover after 15 month run with model 002 (flat continent spin-up experiment).

20. January snow cover after 20 month run with model 002.

21. Mean January temperature (K) of layer 1000-850 mb for 18 months (3-20) of model run 002.

22. Mean January sea-level pressure (mb) for 18 months (3-20) of model run 002.

23. Mean January geopotential height (m) of 500 mb level for 18 months (3-20) of model run 002.

24. Observed climatological mean January sea-level pressure field (mb) (from NOAA and NCAR data).

25. Observed climatological mean January 500 mb geopotential height field (m) (from NOAA and NCAR data).

26. Mean daily precipitation rate (mm day^{-1}) in January computed for the 10-th month of the water planet spin-up experiment (000).

27. Mean daily precipitation rate (mm day^{-1}) in January computed for the 20-th month of the flat continent experiment (002)

28. Mean daily precipitation rate (mm day^{-1}) in January computed for the 25-th month of model run 002.

29. January snow cover after 14 month run with model 003 (mountain experiment).

30. Mean January surface temperature field (^{o}C) for 14-th month of model run 003.

Figures (Cont'd.)

31. Mean daily precipitation rate (mm day^{-1}) in January for 20 months (6-25) of model run 002 (flat continents).

32. Mean daily precipitation rate (mm day^{-1}) in January for 20 months (6-25) of model run 003 (mountains).

33. Mean surface temperature field (^{o}C) in January for 20 months (6-25) of model run 002 (flat continents).

34. Mean surface temperature field (^{o}C) in January for 20 months (6-25) of model run 003 (mountains).

35. Mean meridional cross-section of zonal wind (10^{-1} ms^{-1}) in January for 13 months (3-15) of model run 000 (water planet, spin-up).

36. Mean meridional cross-section of zonal wind (10^{-1} ms^{-1}) in January for 20 months (6-35) of model run 002 (flat continents).

37. Mean meridional cross-section of zonal wind (10^{-1} ms^{-1}) in January for 20 months (6-25) of model run 003 (mountains).